NORTHWESTERN UNIVERSITY

Mathematical Modeling of the Formation of Surface Nanostructures in Thin Solid Films

A DISSERTATION

SUBMITTED TO THE GRADUATE SCHOOL

IN PARTIAL FULFILLMENT OF THE REQUIREMENTS

for the degree

DOCTOR OF PHILOSOPHY

Field of Applied Mathematics

By

Margo S. Levine

EVANSTON, ILLINOIS

June 2007

ABSTRACT

Mathematical Modeling of the Formation of Surface Nanostructures in Thin Solid Films

Margo S. Levine

The self-assembly of quantum dots (QDs) in thin solid films is an important area of nanotechnology with many relevant applications. In the present thesis, three problems related to the growth and self-assembly of QDs are investigated.

In Chapter 1, a new instability mechanism for the formation of QDs associated with strong surface energy anisotropy coupled with wetting interactions between the film and the substrate is proposed. A nonlinear anisotropic evolution equation describing the shape of a thin solid film deposited on a solid substrate is derived and the stability analysis of a planar film is performed. The wetting interactions are found to change the instability spectrum from long-wave to short-wave, leading to the possibility of the formation of stable regular arrays of QDs. Near the short-wave instability threshold, it is found that the formation of stable hexagonal arrays of QDs is possible.

In Chapter 2, the effects of wetting interactions on another mechanism of QD formation are investigated. This mechanism is associated with the Asaro-Tiller-Grinfeld instability that releases epitaxial stress caused by the lattice mismatch between the film and the

substrate. The elasticity problem in the long-wave approximation is solved and a nonlocal integro-differential equation governing the evolution of the film surface is derived. It is shown that wetting interactions can change instability spectrum from the spinodal decomposition type to the Turing type leading to the possibility of pattern formation. For typical semiconductor systems, hexagonal arrays of QDs are found to be unstable as a result of a subcritical bifurcation. It is shown that the QDs coarsen after formation and the coarsening dynamics are studied by numerical simulations.

In Chapter 3, the formation of an epitaxial film by molecular beam epitaxy (MBE), which precedes the formation of QDs, is investigated. The Burton-Cabrera-Frank theory for the growth of a stepped crystal surface is studied when the adatom diffusion is anomalous (Lévy flights). The step-flow velocity is obtained as an eigenvalue of the corresponding superdiffusion problem described by a fractional partial differential equation. The crystal surface growth rate is found as a function of the terrace length and the anomalous diffusion exponent.

Acknowledgements

I cannot overemphasize my gratitude to my Ph.D advisor, Sasha Golovin. He has been a thoroughly attentive and patient mentor as well as a supportive friend.

I thank Professors Volodia Volpert and Steve Davis for serving on my thesis committee as well as Professor Peter Voorhees for his insight and advice on matters of materials sciences.

I am grateful to my friends and colleagues for making the ESAM department both a productive and fun environment to learn and grow like a plant. I would like to thank Lael Fisher for recruiting me to play water polo, Christine Sample for rallying with me for pudding justice, Gogi Singh for instructing me in the wondrous workings of Mathematica and Liam Stanton for being—among other things—a very good officemate. I also want to thank Joanna Bieri for a quasi-bottomless bowl of cereal and for being such a dear friend.

I am indebted to the ESAM staff for helping me with matters administrative and otherwise, and particularly to Beth Siculan for making sure I filled out all the necessary graduation paperwork.

Thank you Anna Golovin for many delicious meals and for lovely conversations, and thank you Krokopytch (the Boss) whose Russian spelling is still a mystery to me.

I want to thank my family, both immediate and extended. I would like to thank my parents, Howard and Elyse, for being such inspiring and supportive figures in my life.

I would also like to thank my brother Joe and sister Marina for discussion of obscure medical conditions at the dinner table.

Lastly, I would like to thank Rafael Jaramillo, my husband, my love. IPYWRMR-GOFPUWAMSTPY.

Table of Contents

List of Figures

CHAPTER 1

Introduction

The formation of quantum dots has received significant attention in recent years due to their potential applications in a wide range of industrial processes from the fabrication of biological dyes to the development of new solid-state lasers. One feature of quantum dots is that they can form spontaneously, or self-assemble, as the result of an instability when a thin film of one solid material is deposited onto a substrate of another solid material. The main physical effects that govern this instability are elastic interactions, surface energy, and wetting interactions between the film and the substrate. In this thesis, we investigate two distinct instability mechanisms that may lead to the self-assembly of quantum dots. In Chapter 2, we discuss a stress-free mechanism that is driven by strong surface-energy anisotropy and wetting interactions between the film and the substrate. In Chapter 3, we study the coupling of wetting interactions with epitaxial stress that occurs as a result of lattice mismatch between the film and the substrate.

The self-assembly of quantum dots studied in Chapters 2 and 3 occurs in an initially planar crystalline film. Chapter 4 is devoted to the investigation of the deposition process itself, namely, to the growth of an epitaxial film. We study the step-flow growth of a crystalline surface by molecular beam epitaxy (MBE) in the case when the surface diffusion of adatoms is anomalously fast and described by Lévy flights. As a result, we formulate a Lévy flight analog of the Burton, Cabrera, and Frank theory for step-flow growth.

CHAPTER 2

Faceting Instability in the Presence of Wetting Interactions: A Mechanism for the Formation of Quantum Dots

2.1. Introduction

The formation of quantum dots in epitaxially grown thin solid films has been attracting attention as a very promising area of nanotechnology that can lead to a new generation of electronic devices. It is generally understood that the main mechanism of the formation of quantum dots in thin solid films on solid substrates is the Asaro-Tiller-Grinfeld (ATG) instability [**1**, **2**] that releases epitaxial elastic stresses in the film caused by the crystal lattice mismatch between the film and the substrate [**3**–**8**]. At the same time, other mechanisms can also play an important role in the formation of surface structures during epitaxial growth; two such mechanisms are faceting instability of a thermodynamically unstable surface caused by strong surface-energy anisotropy and slope-dependent surface currents caused by the Schwöbel effect [**9**–**12**].

The characteristic feature of these mechanisms is that they produce long-wave instabilities of the film surface leading to the formation of mounds that usually coarsen in time, with larger islands growing at the expense of smaller ones [**13**]. At the same time, the formation of a system of islands with almost uniform size has been observed [**14**]. Several mechanisms have been identified that can terminate the coarsening process. One

mechanism is a balance between the surface and elastic energies that can lead to the formation of uniform-size islands as a preferred configuration having minimal energy [**4**, **15**]. Another dynamic mechanism is associated with the normal growth of the interface, e.g., by evaporation-condensation or due to the presence of a diffusion boundary layer typical of chemical vapor deposition. The normal growth introduces convective effects in the evolution of the interface that compete with the coarsening process by sustaining ridges and corners of the faceted mounds [**16**–**18**]. However, when the growth stops, further annealing will cause coarsening of the surface structures. Recently, an additional mechanism that can terminate coarsening of the surface structures has been identified. This mechanism is based on wetting interactions between the film and the substrate [**19**, **20**]. It has been shown that wetting interactions can change the spectrum of the ATG instability [**20**–**23**], or surface instability cased by the Schwöbel effect [**24**], and lead to the selection of a finite wavelength near the instability threshold and therefore to the possibility of the formation of permanent spatially regular patterns [**20**]. In this case, spatially regular arrays of dots (or pits) are formed as the result of the nonlinear dynamics near the instability threshold, and the corresponding steady state can be considered as having a local energy minimum. The formation of spatially regular arrays of dots has been investigated for the case of the ATG instability accompanied by wetting interactions between the film and the substrate [**19**, **20**]. The interplay between the film-substrate wetting interactions and the *faceting instability* caused by anisotropic surface energy has not yet been studied. In this chapter, we investigate this coupling and show that, even in the absence of epitaxial stresses, wetting interactions can terminate coarsening and lead to

the formation of permanent regular arrays of quantum dots, as well as spatially localized dots, thus providing a new route for quantum-dot fabrication.

2.2. Problem Statement

Consider a thin solid film grown on a solid substrate where the lattice mismatch between two materials is negligible, the surface energy γ is strongly anisotropic, the film wets the substrate, and the film is thin enough for the wetting interaction energy to affect the chemical potential of the film. Let us also assume that the substrate determines the initial crystallographic orientation of the free surface of the growing film. We assume that *in the absence of the substrate*, or when the film is thick enough so that it does not "feel" the substrate, this orientation would be in the range of "forbidden orientations." We consider only high-symmetry orientations such as [001] and [111]. For these orientations, the forbidden orientation of the growing surface implies that the surface stiffness tensor [**25**, **26**],

$$\tilde{\gamma}_{\alpha\beta} = \gamma\delta_{\alpha\beta} + \frac{\partial^2\gamma}{\partial\theta_\alpha\partial\theta_\beta} \tag{2.1}$$

is diagonal and has two equal negative components,

$$\tilde{\gamma}_{11} = \tilde{\gamma}_{22} \equiv -\sigma < 0, \tag{2.2}$$

where $\theta_{\alpha,\beta}$ are the surface angular coordinates and $\delta_{\alpha\beta}$ is the Kroneker delta. In the absence of wetting interactions between the film and the substrate, such a surface is thermodynamically unstable and exhibits spontaneous formation of pyramidal "faceted" structures that coarsen in time [**16**, **18**]. The film would decompose into faceted islands

and exhibit the Volmer-Weber growth, rather than the Stranski-Krastanov one. However, as we will show, the presence of wetting interactions can *suppress* this instability, or qualitatively change it, so that it would lead to the Stranski-Krastanov growth in the form of spatially regular arrays of islands connected by a thin wetting layer.

The continuum evolution of the film free surface can be described by the classical surface-diffusion equation

$$v_n = \mathcal{D}\nabla_s^2\mu, \tag{2.3}$$

where v_n is the normal surface velocity, $\mathcal{D} = D_S S_0 \Omega_0 V_0/(RT)$ (D_S is the surface diffusivity, S_0 is the number of atoms per unit area on the surface Ω_0 is the atomic volume, V_0 is the molar volume of lattice cites in the film, R is the universal gas constant, T is the absolute temperature) [**27**] and

$$\mu = \frac{\delta \mathcal{F}}{\delta h} \tag{2.4}$$

is the chemical potential, the variational derivative of the free energy, $\mathcal{F}$, with respect to the shape of the film surface, $h(x, y, t)$. The surface Laplace operator, ∇_s^2, is given by

$$\begin{aligned} \nabla_s^2 &= \frac{1}{1+h_x^2+h_y^2}\left[(1+h_y^2)\partial_x^2 - 2h_x h_y \partial_x\partial_y + (1+h_x^2)\partial_y^2\right] \\ &- \frac{1}{(1+h_x^2+h_y^2)^2}\left[(1+h_y^2)h_{xx} - 2h_x h_y h_{xy} + (1+h_y^2)h_{xx}\right](h_x\partial_x + h_y\partial_y), \end{aligned} \tag{2.5}$$

where $\partial_{x,y}$ indicates partial differentiation with respect to x, y, and $h_{x,y} \equiv \partial_{x,y} h$.

In the absence of elastic stresses and wetting interactions between the film and the substrate, we have

$$\mathcal{F} = \int \left[\mu_0 h + I(h_x, h_y) + \frac{1}{2}\nu(\Delta h)^2 \right] dx\, dy, \tag{2.6}$$

where μ_0 is the volume part of the free energy (μ_0 is the constant chemical potential of a planar film), $I = \gamma(h_x, h_y)\sqrt{1 + (\nabla h)^2}$ is the weighted anisotropic surface energy that depends on the local surface slope, and ν is the regularization coefficient that measures the energy of edges and corners [**16**, **28**, **29**] (for simplicity, we write this term in the small-slope approximation that will be further employed in this chapter). The free energy (2.6) gives the chemical potential

$$\mu = \mu_0 + \mu_\gamma \equiv \mu_0 + \tilde{\gamma}_{\alpha\beta} C_{\alpha\beta} + \nu \Delta^2 h, \tag{2.7}$$

where $C_{\alpha\beta}$ is the surface curvature tensor.

In the presence of wetting interactions between the film and the substrate, the film chemical potential μ strongly depends on the film thickness h for $h \sim \delta_w$, where δ_w is the characteristic wetting length, and $\mu \to \mu_0$ for $h \gg \delta_w$. In this case, the film free energy can be written as

$$\mathcal{F} = \int \left[f\left(h, h_x, h_y\right) + \frac{1}{2}\nu(\Delta h)^2 \right] dxdy \tag{2.8}$$

where $f(h, h_x, h_y) \to \mu_0 h + I(h_x, h_y)$ for $h \gg \delta_w$. The *wetting* part of the free energy can then be defined as

$$\mathcal{F}_w = \int \left[f\left(h, h_x, h_y\right) - \mu_0 h - I(h_x, h_y) \right] dxdy. \tag{2.9}$$

We will consider the following two models for wetting interactions between the film and the substrate. The first, a *two-layer wetting model*, where the wetting interactions between the film and the substrate are described as a thickness-dependent surface energy of the film, $\gamma(h)$. This dependence is usually taken to be [**30**]

$$\gamma(h) = \gamma_f + (\gamma_s - \gamma_f) \exp(-h/\delta_w), \tag{2.10}$$

where $\gamma_s = const$ is the surface energy of the substrate in the absence of the film, γ_f is the surface energy of the film free surface far from the substrate, and δ_w is the characteristic wetting length. This model is consistent with *ab initio* calculations [**31**, **32**]. For anisotropic film surface energy,

$$\gamma_f = \gamma_f^0 [1 + \varepsilon(h_x, h_y)], \tag{2.11}$$

where $\gamma_f^0 = const$ and $\varepsilon(h_x, h_y)$ is the anisotropy function that depends on the orientation of the film surface. Thus, in this model, the free energy density in (2.8) is $f(h, h_x, h_y) = \gamma(h, h_x, h_y)\sqrt{1 + |\nabla h|^2}$, and the chemical potential is computed as $\mu = \mu_\gamma + \mathcal{W}$, where μ_γ is defined by (2.7) and

$$\mathcal{W} = \frac{\frac{\partial \gamma}{\partial h} - \left[\frac{\partial^2 \gamma}{\partial h \partial h_x} h_x + \frac{\partial^2 \gamma}{\partial h \partial h_y} h_y \right] (1 + |\nabla h|^2)}{\sqrt{1 + |\nabla h|^2}}. \tag{2.12}$$

Note that in this case $\tilde{\gamma}_{\alpha\beta}$ in μ_γ depends on h. The second wetting model, a *glued wetting-layer model*, considers isotropic wetting free energy, additive to the anisotropic surface energy, yielding $\mu = \mu_\gamma + \mathcal{W}$, with μ_γ defined by (2.7) and $\mathcal{W}$ being an exponentially decaying function of h that has a singularity as $h \to 0$:

$$\mathcal{W} = -w \left(\frac{h}{\delta_w} \right)^{-\alpha_w} \exp(-h/\delta_w). \tag{2.13}$$

Here, δ_w is the characteristic wetting length, $w > 0$ characterizes the "strength" of the wetting interactions, and $\alpha_w > 0$ characterizes the singularity of the wetting potential as $h \to 0$. This singularity is a simple continuum phenomenological model of a very large potential barrier for removal of an ultra-thin (possibly monolayer) wetting layer that persists between surface mounds during Stranski-Krastanov growth process [**24**, **33**, **34**]. We are not aware of experimental studies in which the wetting interaction potential has been measured, and the glued wetting-layer model is a reasonable approximation for the purpose of our analysis.

Thus, in the small-slope approximation and for high-symmetry orientations, the surface chemical potential in both of these wetting models have the same form

$$\mu = \mu_\gamma^0 + \mathcal{W}, \tag{2.14}$$

where $\mu_\gamma^0 = \mu_\gamma(h_0)$ is defined by (2.7) and evaluated at the initial film thickness h_0, and the part of the chemical potential due to wetting can be expanded as

$$\mathcal{W} = W_0(h) + W_2(h)(\nabla h)^2 + W_3(h)\nabla^2 h + \ldots, \tag{2.15}$$

where $W_{0,2,3}(h)$ are smooth functions, rapidly (exponentially) decaying with increasing h, $W_3(h_0) = 0$, and $2W_2 = dW_3/dh$ (due to Eq. (2.4)). In the small slope approximation, and in the particular cases of high-symmetry orientations ([001] or [111]) of a crystal with cubic symmetry, the evolution equation (2.3) for the film thickness can be written in the following form:

$$\frac{\partial h}{\partial t} = \mathcal{D}\Delta\left[\sigma\Delta h + \nu\Delta^2 h - \Gamma_{ijk}[h] + W_0(h) + W_2(h)(\nabla h)^2 + W_3(h)\Delta h\right], \tag{2.16}$$

where the functions $W_{0,2,3}(h)$ are determined by the type of wetting interactions model. In Eq. (2.16), $\Gamma_{ijk}[h]$ is a nonlinear differential operator that depends on the orientation of the film surface. To determine $\Gamma_{ijk}[h]$ for a particular surface, we write the general free energy density

$$\mathcal{G}_{ijk} = b_1 h_x^3 + b_2 h_x^2 h_y + b_3 h_x h_y^2 + b_4 h_y^3 + c_1 h_x^4 + c_2 h_x^3 h_y + c_3 h_x^2 h_y^2 + c_4 h_x h_y^3 + c_5 h_y^4, \tag{2.17}$$

and apply the appropriate lattice symmetry conditions. For the [001] surface, Eq. (2.17) must be invariant with respect to rotations by $\pi/2$, as well the transformations from $x \to -x, y \to -y$, and $x \to y$, from which we obtain

$$\mathcal{G}_{100} = b_2 h_x^2 h_y^2 + c_1(h_x^4 + h_y^4). \tag{2.18}$$

The resulting chemical potential, after letting $2\,b_2 \to b$ and $12\,c_1 \to a$, is

$$\Gamma_{001} = (a h_x^2 + b h_y^2) h_{xx} + (b h_x^2 + a h_y^2) h_{yy} + 4 b h_x h_y h_{xy}. \tag{2.19}$$

In a similar manner, $\Gamma_{ijk}[h]$ must be invariant with respect to rotations by $2\pi/3$ as well as the transformations $y \to -y, b \to -b$. Thus, we have

$$\begin{aligned}(2.20)\quad \Gamma_{111} &= a(h_x^2 h_{xx} + h_y^2 h_{yy} + 2h_x h_y h_{xy}) + \frac{a}{3}\left(h_y^2 h_{xx} + h_x^2 h_{yy} - 2h_x h_y h_{xy}\right) \\ &+ b[(h_{xx} - h_{yy})h_y + 2h_{xy}h_x].\end{aligned}$$

Note that Eq. (2.16) with the nonlinear operators Γ_{ijk} defined by (2.19) and (2.20) can be written in the variational form

$$(2.21)\qquad \frac{\partial h}{\partial t} = \mathcal{D}\nabla^2\left(\frac{\delta \mathcal{F}}{\delta h}\right),$$

where $\mathcal{F} = \int F dx\, dy$, and

$$(2.22)\qquad F = -\frac{\sigma}{2}(\nabla h)^2 + \frac{\nu}{2}(\Delta h)^2 + \mathcal{G}_{ijk} + \int W_0(h)dh - \frac{1}{2}W_2(h)(\nabla h)^2,$$

is the free energy density with

$$(2.23)\qquad \mathcal{G}_{001} = \frac{a}{12}(h_x^4 + h_y^4) + \frac{b}{2}h_x^2 h_y^2,$$

$$(2.24)\qquad \mathcal{G}_{111} = \frac{a}{12}(\nabla h)^4 + \frac{b}{6}(3h_x^2 h_y - h_y^2).$$

In the following sections, we investigate the stability and nonlinear dynamics of the solid-film surface governed by Eq. (2.16).

2.3. Faceting Instability in the Presence of Wetting Interactions

We consider infinitesimal perturbations of a planar film surface, $h = h_0 + \tilde{h}e^{i\mathbf{k}\cdot\mathbf{x}+\omega t}$, and linearize Eq. (2.16) to obtain the following dispersion relation between the perturbation

growth rate ω and the wave vector $\mathbf{k}$:

$$\omega = \mathcal{D}(-W_{01}k^2 + \sigma k^4 - \nu k^6), \tag{2.25}$$

where $k = |\mathbf{k}|$ and

$$W_{01} = \left(\frac{\partial W_0}{\partial h}\right)_{h=h_0}. \tag{2.26}$$

One can see that if the film wets the substrate, i.e., when $W_{01} > 0$, the wetting interactions suppress the long-wave faceting instability caused by the surface-energy anisotropy. The instability occurs only for

$$\frac{\sigma}{4\nu W_{01}} > 1, \tag{2.27}$$

i.e., if either the wetting interaction is less than the threshold value, $W_{01} < W_{01}^c \equiv \sigma^2/(4\nu)$, or the surface stiffness is larger than the threshold value, $\sigma > \sigma_c \equiv 2\sqrt{W_{01}\nu}$. At the instability threshold, the wavelength of the unstable perturbations λ is *finite*, $\lambda = \lambda_c = 2\pi/k_c$, where

$$k_c = \sqrt{\frac{\sigma}{2\nu}}. \tag{2.28}$$

Typical dispersion curves defined by Eq. (2.25) are schematically shown in Fig. 2.1. Note that the critical wave number at the threshold does not depend on the wetting potential and is determined only by the surface stiffness and the energy of edges and corners. For the parameter values typical of semiconductors like Si or Ge, with the surface energy $\gamma \sim 2.0$ J m^{-2}, surface stiffness $\sigma \sim 0.2$ J m^{-2}, the lattice spacing $a_0 \sim 0.5$ nm and the

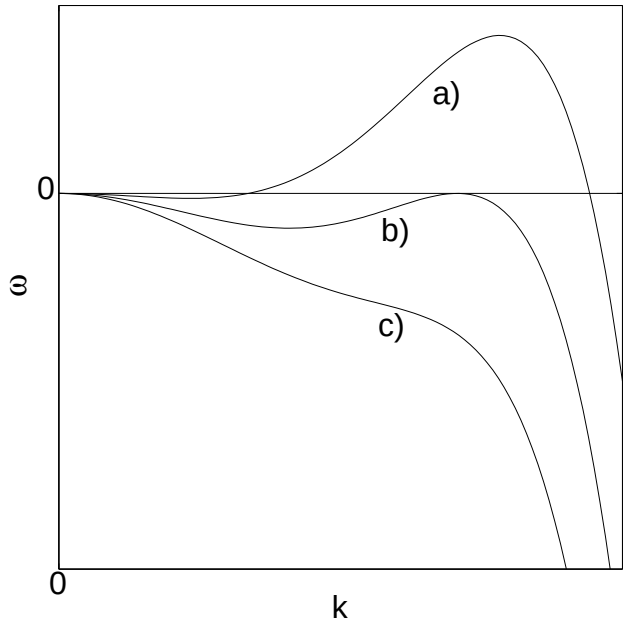

Figure 2.1. Sketch of dispersion curves defined by Eq. (2.25) for (a) $\sigma^2/(4\nu W_{01}) > 1$, (b) $\sigma^2/(4\nu W_{01}) = 1$, and (c) $\sigma^2/(4\nu W_{01}) < 1$.

regularization parameter $\nu \sim \gamma a_0^2 \sim 5.0 \cdot 10^{-19}$ J, the wavelength of the structure at the onset of instability is 14 nm.

Thus, in the presence of wetting interactions between the film and the substrate, the faceting instability becomes *short-wave*. This is qualitatively different from the case of faceting instability in the absence of wetting interactions. In the latter, the instability is *long-wave*, i.e., all perturbations whose wavelengths are larger than a certain threshold are unstable. In other words, wetting interactions with the substrate change the faceting instability from the spinodal decomposition type [**29**, **35**] to the Turing type [**36**], thus leading to the possibility of changing the system evolution from Ostwald ripening (coarsening) to the formation of spatially regular patterns. The latter is studied in the next sections.

2.4. Formation of Surface Structures: 1+1 Case

In this section, we investigate the nonlinear evolution of surface structures resulting from the faceting instability in the presence of wetting interactions with the substrate in the 1+1 case of a two-dimensional film with a one-dimensional surface. In this case, the evolution equation (2.16) for the shape of the film surface, after the rescaling $x \to (\nu/\sigma)^{1/2}x$, $t \to [\nu^2/(\mathcal{D}\sigma^3)]t$, $h \to (\nu/a)^{1/2}h$, becomes

$$\frac{\partial h}{\partial t} = \left[h_{xx} + h_{xxxx} - h_x^2 h_{xx} + w_0(h) + w_2(h)h_x^2 + w_3(h)h_{xx}\right]_{xx}, \tag{2.29}$$

where $w_{0,2,3}(h)$ are the rescaled functions $W_{0,2,3}(h)$, respectively ($w_3(h_0) = 0$, $2w_2 = dw_3/dh$). In this scaling, the instability occurs for $(\partial w_0/\partial h)_{h=h_0} \equiv w_{01} < \frac{1}{4}$ at the wave number $k_c = \sqrt{2}/2$. We now investigate the evolution of structures near the instability threshold by means of weakly nonlinear analysis.

Let us consider $w_{01} = \frac{1}{4} - 2\epsilon^2$, $\epsilon \ll 1$, introduce the long-scale coordinate $X = \epsilon x$ and the slow time $T = \epsilon^2 t$, and expand

$$\begin{aligned} \tilde{h} &= h - h_0 = \epsilon\left[A(X,T)e^{ik_c x} + c.c.\right] \\ &+ \epsilon^2\left[A_2(X,T)e^{2ik_c x} + B(X,T) + c.c.\right] + \cdots, \end{aligned} \tag{2.30}$$

$$w_0(h) = w_{00} + w_{01}\tilde{h} + w_{02}\tilde{h}^2 + w_{03}\tilde{h}^3 + \cdots, \tag{2.31}$$

$$w_2(h) = w_{20} + w_{21}\tilde{h} + \cdots, \tag{2.32}$$

$$w_3(h) = w_{31}\tilde{h} + w_{32}\tilde{h}^2 + \cdots, \tag{2.33}$$

where $w_{31} = 2w_{20}$ and $w_{32} = w_{21}$. We substitute (2.31)- (2.33) into Eq. (2.29) to obtain the corresponding problems in successive orders of ϵ. From the problem at second order, one finds

$$A_2 = \frac{2}{9}(3w_{20} - 2w_{02})A^2. \tag{2.34}$$

From the solvability condition at the third order, we obtain the evolution equation for the complex amplitude of the unstable, spatially periodic mode, $A(X,T)$. The problem at the fourth order yields the evolution equation for the real amplitude $B(X,T)$ of the zero mode associated with conservation of mass. Together, the two equations form the following system of coupled equations:

$$\begin{aligned} A_T &= A + A_{XX} - \lambda_0|A|^2A + sAB, \\ B_T &= \frac{1}{4}B_{XX} - 2s\left(|A|^2\right)_{XX}, \end{aligned} \tag{2.35}$$

where

$$\lambda_0 = \frac{1}{8} - \frac{1}{9}(3w_{20} - 2w_{02})^2 - \frac{1}{2}w_{21} + \frac{3}{2}w_{03}, \tag{2.36}$$

$$s = \frac{1}{2}w_{20} - w_{02}. \tag{2.37}$$

We now analyze the stability of the periodic stationary solution of system (2.35), $A_0 = \lambda_0^{-1/2}$, $B = 0$, in the form of rolls. We let

$$A(X,T) = A_0 + A_1(X,T)e^{\sigma T + iqX} + A_2(X,T)e^{\sigma^* T - iqX}, \tag{2.38}$$

$$B(X,T) = B_1(X,T)e^{\sigma T + iqX} + B_1^*(X,T)e^{\sigma^* T - iqX}, \tag{2.39}$$

where $B_1^*(X,T)$ and σ^* denote the complex conjugates of $B_1(X,T)$ and σ, respectively, and linearize system (2.35) in $A(X,T)$ and $B(X,T)$. The linearization results in the homogeneous system of equations for $A_1(X,T)$, $A_2^*(X,T)$, and $B_1(X,T)$,

$$\begin{bmatrix} \sigma+q^2+1 & 1 & -sA_0 \\ 1 & \sigma+q^2+1 & -sA_0 \\ sA_0 & sA_0 & -\sigma-\frac{1}{4}q^2 \end{bmatrix} \begin{pmatrix} A_1 \\ A_2^* \\ B_1 \end{pmatrix} = \begin{pmatrix} 0 \\ 0 \\ 0 \end{pmatrix}, \tag{2.40}$$

with the solvability condition

$$(\sigma+q^2)\left[4\sigma^2+(8+5q^2)\sigma+q^4+2q^2-8A_0^2s^2\right]=0. \tag{2.41}$$

The greatest disturbances occur when $q \to 0$. Thus, the system of amplitude equations (2.35) has a stable, stationary solution, $A_0=\lambda_0^{-1/2}$, $B=0$, corresponding to a spatially periodic pattern (array of dots) if [**20**, **37**]

$$\lambda_0 > 8s^2 = 2(w_{20}-2w_{02})^2. \tag{2.42}$$

Condition (2.42) defines a region in the parameter space in which one can observe the formation of stable periodic arrays of dots. First, consider a *glued-layer* wetting potential defined by (2.13). From condition (2.27), one finds that the planar film surface becomes unstable with respect to periodic structures for

$$-\frac{\sigma^2\delta_w}{w\nu} > 4(\alpha_w+\zeta)\zeta^{-(\alpha_w+1)}e^{-\zeta}, \tag{2.43}$$

where $\zeta = h_0/\delta_w$. Since, for the *glued-layer* wetting potential, $w_2(h) = w_3(h) \equiv 0$, one obtains from (2.42) and (2.43) that a near-threshold periodic surface structure is stable if

$$\frac{a\delta_w^2}{\nu} > f(\zeta, \alpha_w), \tag{2.44}$$

where

$$\begin{aligned} f(\zeta, \alpha_w) &= [18\zeta^2(\zeta+\alpha)^2]^{-1}[10\zeta^3 + 40\alpha_w\zeta^3 \\ &+ \alpha_w(11+60\alpha_w)\zeta^2 + 2\alpha_w(20\alpha_w^2 + 11\alpha_2 - 9)\zeta \\ &+ \alpha_w^2(1-\alpha_w^2+11\alpha_w+1)]. \end{aligned} \tag{2.45}$$

Conditions (2.43) and (2.44) are shown in Fig. 2.2.

Now consider a *two-layer* wetting potential defined by (2.10) with

$$\gamma_f = \gamma_f^0[1 + \varepsilon\cos 4(\theta_0 + \theta)], \tag{2.46}$$

where $\theta = \arctan(h_x)$ and θ_0 corresponds to the orientation of the planar surface of the film, parallel to the substrate; for the high-symmetry orientations [01] and [10], $\theta_0 = 0, \pi/4$, respectively. It is convenient to introduce the following dimensionless parameters:

$$\Gamma = \frac{\gamma_{f0}}{\gamma_s}(15\varepsilon - 1), \quad \zeta = \frac{h_0}{\delta_w}, \quad \tilde{\varepsilon}_1 = \frac{\varepsilon+1}{15\varepsilon-1}, \quad \tilde{\varepsilon}_2 = \frac{95\varepsilon-1}{15\varepsilon-1}. \tag{2.47}$$

The film wets the substrate if $\Gamma < \tilde{\varepsilon}_1^{-1}$ or $\gamma_s/\gamma_{f0} > \varepsilon + 1$. In this case, the nonlinear anisotropy coefficient a in Eq. (2.16) is always positive. The faceting instability requires

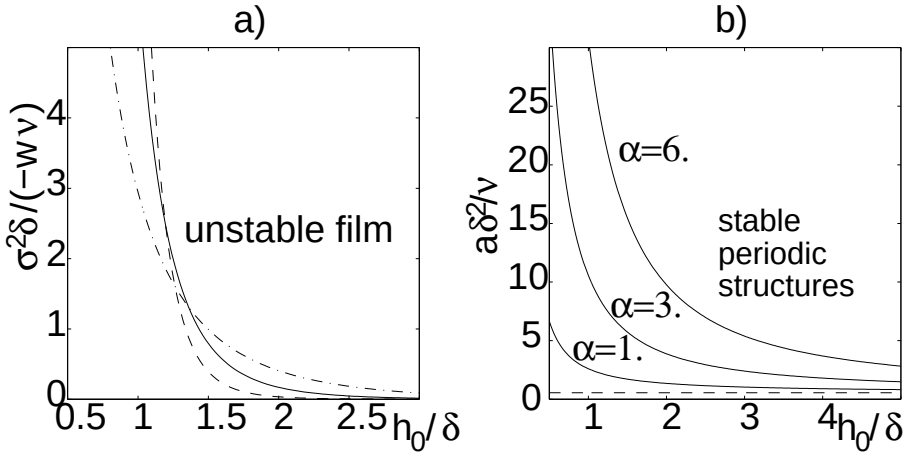

Figure 2.2. (a) Parameter regions where a planar film surface is unstable (above the corresponding curves) for $\alpha_w = 3.0$ (solid line) and $\alpha_w = 1.0$ (dashed-dotted line). (b) Parameter regions where weakly nonlinear periodic surface structures are stable (above corresponding curves) for different values of α_w.

a negative surface stiffness that can achieved if $15\varepsilon - 1 > 0$, and

$$\zeta > \ln(1 + \Gamma^{-1}). \tag{2.48}$$

This instability threshold condition (2.27) gives

$$\frac{\gamma_s \delta_w^2}{\nu} \geq \frac{4e^{\zeta}(1 - \Gamma\tilde{\varepsilon}_1)}{[\Gamma(e^{\zeta} - 1) - 1]^2}. \tag{2.49}$$

The analysis of conditions (2.48) and (2.49) shows that the short-wave instability of the film surface that can lead to pattern formation can occur only if the film thickness is above a threshold value determined by the surface-energy anisotropy and the wetting length,

namely, for

$$h_0 > \delta_w \ln\left[\frac{16\varepsilon}{15\varepsilon - 1}\right]. \tag{2.50}$$

Using (2.42), one can show that the weakly nonlinear periodic structure is stable if

$$\frac{\gamma_s \delta_w^2}{\nu} > f(\zeta, \Gamma, \varepsilon), \tag{2.51}$$

where

$$f = \frac{2}{27}\frac{\Gamma^2(5e^{2\zeta} + 14e^{\zeta} + 35) + 14\Gamma(e^{\zeta} + 5) + 35}{e^{-\zeta}[\Gamma(e^{\zeta} - 1) - 1]^2[\tilde{\varepsilon}_2\Gamma(e^{\zeta} - 1) - 1]} \tag{2.52}$$

The conditions (2.48)-(2.51) allow one to determine regions in the (Γ, ζ) parameter plane where spatially regular surface structures can occur as a result of the thermodynamic instability of the film surface caused by strongly anisotropic surface tension in the presence of wetting interactions described by (2.10). Examples of these regions for different values of the anisotropy parameter ε are shown in Fig. 2.3. The solid curves correspond to condition (2.49), and the dashed curves correspond to condition (2.51). The film is unstable in the regions above the solid curves, and stable periodic structures can form in the region near the solid curve which lies above the dashed curve. One can see that for given values of the surface-energy anisotropy, ε, and $\gamma_s\delta_w/\nu$, the formation of stable periodic structures occurs if the ratio of the initial film thickness to the wetting length is within a certain interval.

Numerical simulations of Eq. (2.29) were performed in [**38**] for the two types of wetting potential. For both wetting potentials, the numerical solutions exhibited the

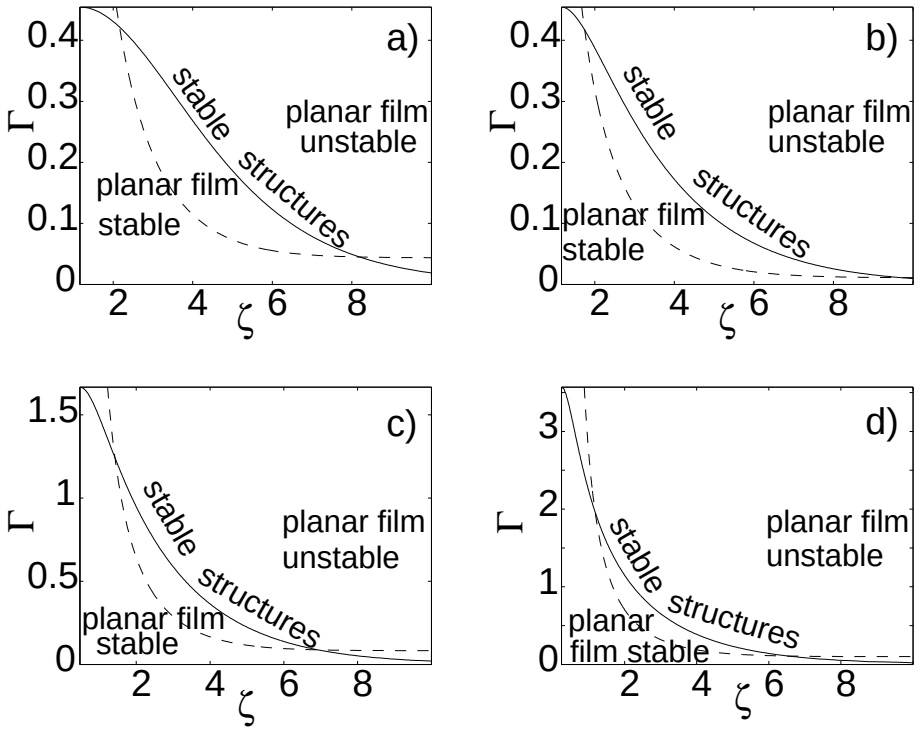

Figure 2.3. (a) Parameter regions where a planar film surface is unstable (above the solid curve) and where stable periodic structures can form near the instability threshold (near the solid curve, above the dashed curve): (a) $\varepsilon = 0.1$, $\gamma_s\delta_w^2/\nu = 0.5$, (b) $\varepsilon = 0.1$, $\gamma_s\delta_w^2/\nu = 2.0$, (c) $\varepsilon = 0.2$, $\gamma_s\delta_w^2/\nu = 0.5$ and (d) $\varepsilon = 0.4$, $\gamma_s\delta_w^2/\nu = 0.5$.

formation of stable periodic structures near the instability threshold in the parameter regime where these structures are stable. Outside of these regimes, or further from the instability threshold, the periodic structures become unstable and exhibit behavior that depends on the type of wetting interactions. For the glued-layer potential, Fig 2.4 shows the stationary solution of Eq. (2.29) as one moves away from the short-wave instability threshold, and Fig 2.5 shows different stages of the coarsening process and the formation of localized islands.

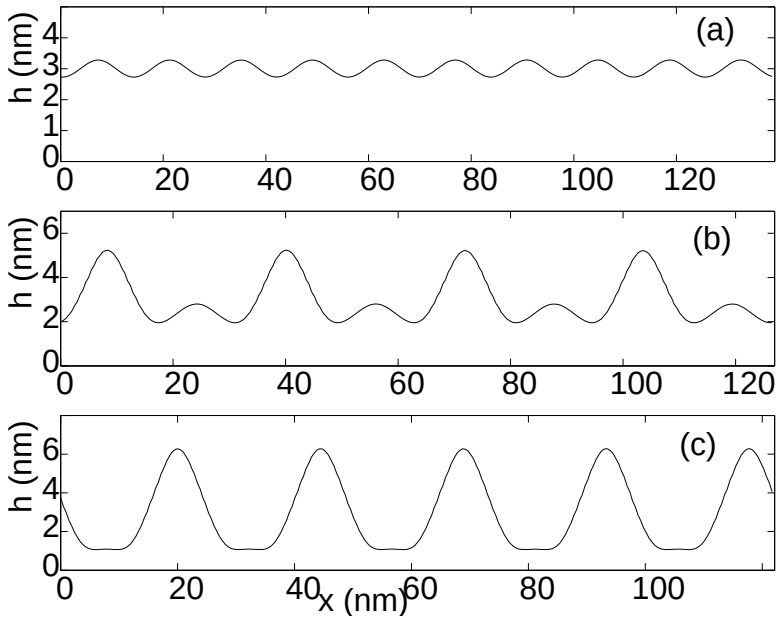

Figure 2.4. Stationary numerical solutions of Eq. (2.29) with the wetting potential (2.13) showing stationary surface structures for $h_0 = 3.0$ nm, ($\zeta = 2.0$), $a = 0.17$ J m^{-2}, and (a) $w = 6.8 \cdot 10^8$ J m^{-3} ($w_{01} = 0.24$), (b) $w = 2.8 \cdot 10^8$ J m^{-3} ($w_{01} = 0.1$), (c) $w = 2.8 \cdot 10^7$ J m^{-3} ($w_{01} = 0.01$).

2.5. Formation of Surface Structures: 2+1 Case

In this section, we investigate the nonlinear evolution of surface structures resulting from the faceting instability of a three-dimensional film with a two-dimensional surface ($2 + 1$ case) in the presence of wetting interactions with the substrate. We consider high-symmetry orientations only, [001] and [111], described by Eq. (2.16).

After the appropriate rescaling, Eq. (2.16) can be written as

$$\frac{\partial h}{\partial t} = \Delta \left[\Delta h + \Delta^2 h - g[h] + w_0(h) + w_2(h)(\nabla h)^2 + w_3(h)\Delta h \right], \tag{2.53}$$

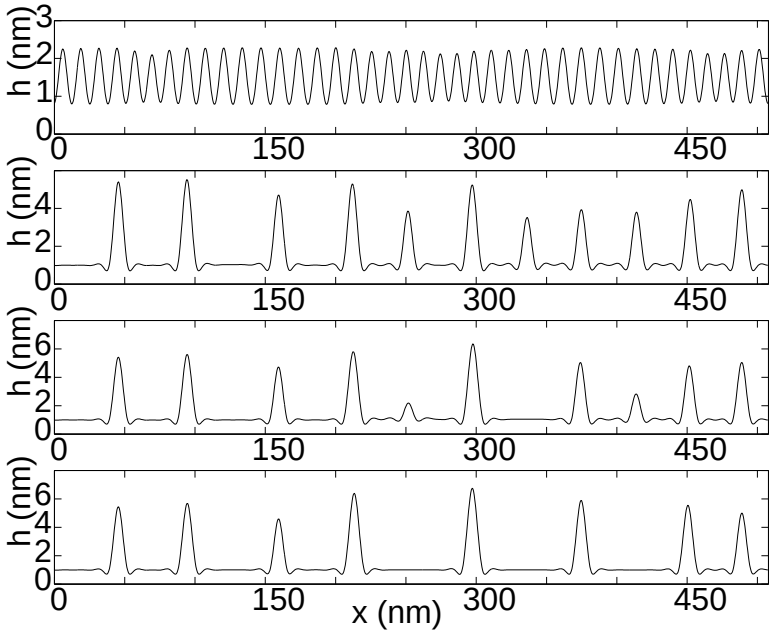

Figure 2.5. Different stages of coarsening of the initial periodic structure, yielding the formation of localized dots divided by a thin wetting layer–the numerical solution of Eq. (2.29) with the wetting potential (2.13) $h_0 = 1,5$ nm, $w = 8.2 \cdot 10^6$ J m^{-3} ($\zeta = 1.0, w_{01} = 0.1$), $a = 0.22$ J m^{-2}.

where the nonlinear differential operator $g[h]$ for the [001] orientation is

$$g_{001} = (h_x^2 + ph_y^2)h_{xx} + (h_y^2 + ph_x^2)h_{yy} + 4ph_x h_y h_{xy}, \tag{2.54}$$

and for the [111] orientation

$$g_{111} = \left(h_x^2 + \frac{1}{3}h_y^2\right)h_{xx} + \left(h_y^2 + \frac{1}{3}h_x^2\right)h_{yy} + \frac{4}{3}h_x h_y h_{xy} + q[(h_{xx} - h_{yy})h_y + 2h_{xy}h_x]. \tag{2.55}$$

Equation (2.53) has a special structure in that the linear operator is isotropic, while the nonlinear operator is anisotropic. The linear growth rate near the instability threshold, thus, does not depend on the wave vector orientation and the resulting dispersion relation is the same as in the 1+1 case, $\omega = -w_{01}k^2 + k^4 - k^6$, with the instability threshold $w_{01} = \frac{1}{4}$

at $k = k_c = \sqrt{2}/2$. It is the nonlinear interaction between the modes that will determine the symmetry of the emerging pattern. This situation is similar to the one considered in Ref. [**39**] where the effect of surface-energy anisotropy on the formation of cellular patterns with different symmetries at a crystal-melt interface caused by morphological instability during directional solidification was studied. Below, we consider the weakly nonlinear analysis near the instability threshold.

Since the linear operator in Eq. (2.53) is isotropic and the nonlinear operator in Eq. (2.53) has a quadratic nonlinearity that breaks the $h \to -h$ symmetry, the preferred pattern near the instability threshold will have a *hexagonal* symmetry. This hexagonal symmetry is caused by the quadratic resonant interaction between three different modes orientation at 120^o with respect to one another and having the same linear growth rate. The specific type of pattern in this case is determined by the phase locking of the three resonant modes that depends on the quadratic resonant interaction coefficient. In order to compute this coefficient, take $w_{01} = \frac{1}{4} - 2\gamma\epsilon$, $\epsilon \ll 1$, introduce the slow time $\tau = \epsilon t$, and use the expansions (2.31)-(2.32), as well as the expansion

$$
\begin{aligned}
(2.56) \qquad h &= \epsilon \sum_{n=1}^{3} A_n(\tau) e^{i\mathbf{k_n}\cdot\mathbf{r}} + \epsilon^2 \sum_{n=1}^{3} B_n(\tau) e^{i\mathbf{k_n}\cdot\mathbf{r}} \\
&+ \epsilon^2 \sum_{n=1}^{3} \left[B_{n,n}(\tau) e^{2i\mathbf{k_n}\cdot\mathbf{r}} + B_{n,n-1}(\tau) e^{i(\mathbf{k_n}-\mathbf{k_{n-1}})\cdot\mathbf{r}} \right] + c.c. + O(\epsilon^3),
\end{aligned}
$$

where $A_n(\tau)$, $B_n(\tau)$, $B_{n,n}(\tau)$ and $B_{n,n-1}(\tau)$ are complex amplitudes (the spatially uniform mode $B_{n,-n}(\tau)$ is missing due to conservation of mass), $\mathbf{r}$ is a vector in the (x, y) plane, $k_n = \sqrt{2}/2$ and $\mathbf{k_1} + \mathbf{k_2} + \mathbf{k_3} = \mathbf{0}$ ($n = 0$ and $n = 3$ correspond to the same mode with the wave vector $\mathbf{k_3}$). Then, the solvability condition for the problem for B_n in the order

ϵ^2 yields the following three evolution equations for the amplitudes $A_{1,2,3}$:

$$\frac{\partial A_1}{\partial \tau} = \gamma A_1 + \alpha A_2^* A_3^*, \tag{2.57}$$

where the other two equations are obtained by the cyclic permutation of the indices in Eq. (2.57). The resonant quadratic interaction coefficient is different for different surface orientations:

$$\alpha^{001} = \frac{3}{4} w_{20} - w_{02}, \tag{2.58}$$

$$\alpha^{111} = \alpha^{001} - i \frac{q}{4\sqrt{2}} \sin(3\phi_0), \tag{2.59}$$

where the angle ϕ_0 characterizes the orientation of the resonant triad $\mathbf{k_1}, \mathbf{k_2}, \mathbf{k_3}$ in the surface plane, $\mathbf{k_1} = (\cos\phi_0, \sin\phi_0)$. Thus, in the case of the [001] surface, the quadratic mode interaction is isotropic, while in the case of the [111] surface, it depends on the pattern orientation within the [111] plane.

For equilateral patterns, $A_n = \rho e^{i\theta_n}$ and using $\alpha = |\alpha| e^{i\delta}$, one obtains from (2.57) the following system of equations for ρ and $\Theta = \theta_1 + \theta_2 + \theta_3$:

$$\frac{\partial \rho}{\partial \tau} = \gamma \rho + |\alpha| \rho^2 \cos(\Theta - \delta), \tag{2.60}$$

$$\frac{\partial \Theta}{\partial \tau} = -3\rho |\alpha| \sin(\Theta - \delta). \tag{2.61}$$

Eq. (2.61) has two critical points: stable, $\Theta = \delta$, and unstable, $\Theta = \pi + \delta$. Thus, the system (2.60) and (2.61) describes an unbounded growth of a pattern given by a function

$$h = \rho[\cos(\mathbf{k_1} \cdot \mathbf{x} + \theta_1) + \cos(\mathbf{k_2} \cdot \mathbf{x} + \theta_2) + \cos(\mathbf{k_3} \cdot \mathbf{x} + \theta_3)], \tag{2.62}$$

in which the phases are locked: $\theta_1 + \theta_2 + \theta_3 = \delta$. If the resonant interaction coefficient is real, then $\delta = 0(\alpha > 0)$ or $\delta = \pi(\alpha < 0)$, and the function (2.62) describes a spatially regular array of hexagons with $h > 0(h < 0)$ in the centers of the hexagons for $\alpha > 0(\alpha < 0)$. Therefore, in the case of the [001] surface when α^{001} is real, one could observe the growth of regular hexagonal arrays of dots for $\alpha^{001} > 0$ or pits for $\alpha^{001} < 0$. Note that for the [001] orientation, the pattern type is determined purely by the details of the wetting potential (the coefficients w_{02} and w_{20}) since, in this case, the anisotropic surface energy enters only through the quartic terms in the free energy functional yielding cubic nonlinear terms in the evolution equation for the surface shape. For example, for a glued wetting potential of type (2.13), $w_{20} = 0$, $\alpha^{001} = w_{02} > 0$, and therefore only the formation of hexagonal arrays of *dots* is possible; an array of pits cannot form.

The situation is different for the [111] orientation when the free-energy functional has anisotropic cubic terms leading to anisotropic quadratic terms in the evolution equation for the surface shape and the complex quadratic resonant interaction coefficient. In this case, the imaginary part of the resonant interaction coefficient depends on the surface-energy anisotropy coefficient, q, and the pattern orientation within the [111] plane (angle ϕ_0). As one can see from (2.60), the most rapidly growing pattern corresponds to the maximum of $|\alpha|$ that is achieved for $\phi_0 = \pi/6$. In this case, one would observe the growth of a pattern described by the function (2.62) with the phases locked at

$$\Theta = \arctan\left[\frac{q/\sqrt{2}}{4w_{02} - 3w_{20}}\right]. \tag{2.63}$$

Examples of patterns corresponding to different values of Θ are shown in Fig. 2.6 (see also Ref. [**39**]). One can see that for intermediate values of Θ, the growing pattern consists

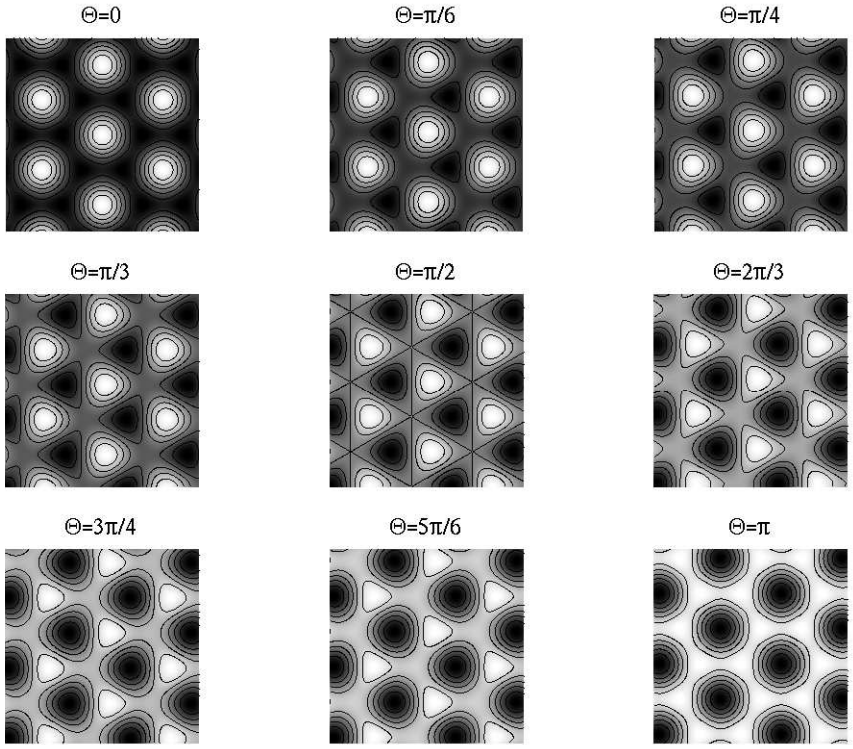

Figure 2.6. Spatial patterns described by Eq. (2.62) with different values of $\Theta = \theta_1 + \theta_2 + \theta_3$.

of a regular hexagonal array of triangular pyramids. Notes that similar hexagonal arrays of triangular pyramids were observed in experiments reported in Ref. [**40**]. Although the physical mechanism of the formation of ordered arrays of triangular pyramids observed in Ref. [**40**] was different (elastic interaction of multiple epitaxial layers), the *nonlinear mechanism* based on the resonant quadratic interaction of unstable modes in the presence of the anisotropy of the [111] is universal and may well be the same in the system studies in Ref. [**40**].

The amplitude equations (2.57) cannot describe the nonlinear stabilization of a growing surface structure and cannot provide conditions for the formation of stable, spatially

regular structures near the instability threshold. In order to obtain such conditions, higher order cubic nonlinear terms in the amplitude equations need to be taken into account. Letting $w_{01} = \frac{1}{4} - 2\gamma\epsilon^2$, $\epsilon \ll 1$, $\tau = \epsilon^2 t$, and using the previous expansions (2.31)-(2.32), (2.56) yields the following evolution equations for the amplitudes A_n at order ϵ^3:

$$\frac{\partial A_n}{\partial \tau} = \gamma A_n + \alpha A_l^* A_m^* - \lambda_0 |A_n|^2 A_n - \lambda(|A_l|^2 + |A_m|^2) A_n, \tag{2.64}$$

with the resonant interaction coefficient α in Eqs. (2.58) and (2.59). The other two equations are obtained by the cyclic permutation of the indices in Eq. (2.64). The self-interaction and cross-interaction Landau coefficients, λ_0 and λ, in Eq. (2.64) are

$$\lambda_0^{001} = \frac{3(1+p)}{32} - \frac{1}{9}(3w_{20} - 2w_{02})^2 + \frac{3w_{03}}{2} - \frac{w_{21}}{2} - \frac{3p-1}{32}\cos(4\phi_0), \tag{2.65}$$

$$\begin{aligned} \lambda^{001} &= \frac{3(1+p)}{32} + 3w_{03} - w_{21} + \frac{3p-1}{32}\cos(4\phi_0) - \frac{\sqrt{3}(3p-1)}{32}\sin(4\phi_0) \\ &- \frac{1}{8}(4w_{02} - 5w_{20})^2 \end{aligned} \tag{2.66}$$

and

$$\lambda_0^{111} = \frac{1}{8} - \frac{q^2}{36}(1 - \cos(6\phi_0)) - \frac{1}{9}(3w_{20} - 2w_{02})^2 + \frac{3w_{03}}{2} - \frac{w_{21}}{2}, \tag{2.67}$$

$$\lambda^{111} = \frac{1}{8} + 3w_{03} - w_{21} - \frac{3q^2}{32}(1 + \cos(6\phi_0)) - \frac{1}{8}(4w_{02} - 5w_{20})^2, \tag{2.68}$$

for the respective [001] and [111] directions. In the presence of the resonant quadratic interaction, the addition of these cubic terms in the amplitude equations near the instability threshold is asymptotically rigorous only if the quadratic interaction coefficient is small, $|\alpha| \sim \epsilon$, which restricts the validity of the weakly nonlinear analysis to a narrow range

of physical parameters. One can see that the Landau cubic interaction coefficients are anisotropic and depend on the pattern orientation in the surface plane [**39**]. The system (2.64) can be written in terms of the Lyapunov function U as

$$\frac{\partial A_n}{\partial T} = -\frac{\partial U}{\partial A_n^*}, \qquad n = 1, 2, 3, \tag{2.69}$$

where

$$\begin{aligned} U(A_n, A_n^*) &= \sum_{n=1}^{3} \left(-\gamma |A_n|^2 + \frac{\lambda_0}{2} |A_n|^4 \right) - \alpha (A_1 A_2 A_3 + A_1^* A_2^* A_3^*) \\ &+ \lambda (|A_1|^2 |A_2|^2 + |A_1|^2 |A_3|^2 + |A_2|^2 |A_3|^2). \end{aligned} \tag{2.70}$$

For equilateral hexagonal patterns,

$$\rho = \frac{\alpha \pm \sqrt{\alpha^2 + 4\gamma(\lambda_0 + 2\lambda)}}{2(\lambda_0 + 2\lambda)}, \tag{2.71}$$

and

$$U(\phi_0) = -3\gamma\rho^2 - 2\alpha\rho^3 + \left(\frac{3\lambda_0}{2} + 3\lambda \right) \rho^4, \tag{2.72}$$

shown in Fig. 2.7 for [001] and [111] surfaces. Minimizing Eq. (2.72) with respect to ϕ_0 gives the preferred orientation in the plane as $\phi_0 \approx 0.4629$, 2.033 and $\phi_0 = 0$, $\pi/3$, $2\pi/3$, π for the respective [001] and [111] surfaces. For each orientation, the angles ϕ_0 are independent of the wetting parameters and have equal minimum values of U. Since the resonant interaction coefficient α is real for the [001] direction, the ϕ_0 correspond to the pattern orientation in the plane. However for the [111] direction, the resonant interaction coefficient is complex with the most rapidly growing pattern at $\phi_0 = \pi/6$ leading to the

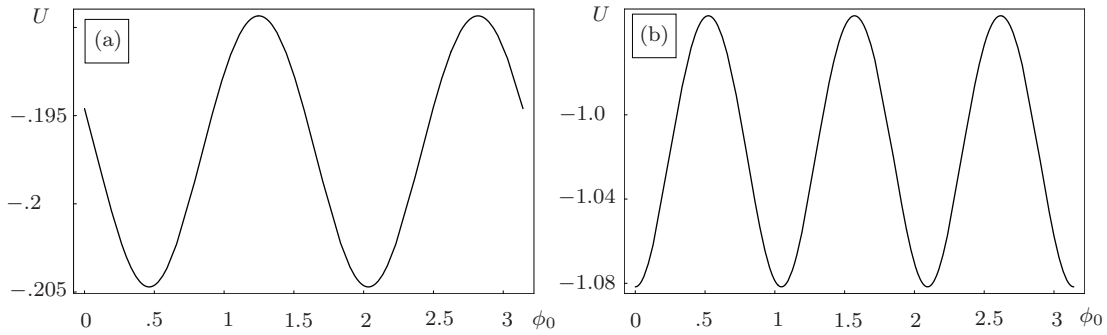

Figure 2.7. Lyapunov functions defined by Eq. 2.72 for (a) [001] and (b) [111] surface orientations

previously discussed phase locking given by Eq. (2.63). Although the pattern will grow at $\phi_0 = \pi/6$, the phase locking will change and the final state of the system will correspond to the minima of U at $\phi_0 = 0$, $\pi/3$, $2\pi/3$, π. The resonant interaction coefficient will be real at these angles and will correspond to hexagonal arrays of either dots or pits.

Numerical simulations of Eq. (2.53) were performed in 2.13 for the [001] and [111] orientations of the film surface with $\Gamma_{ijk}[h]$ defined by (2.19) and (2.20), and for the glued-layer potential defined by (2.13). For sufficiently large surface energy anisotropy, the numerical solutions for the [001] surface exhibited the formation of stable periodic structures as shown in (Fig. 2.8). In the case of the [111] orientation of the film surface, the formation of regular arrays of dots were not observed, even near the instability threshold and for large surface energy anisotropy. Instead, the numerical solutions exhibited the formation of hexagonal arrays of triangular pyramids that coarsened and evolved toward localized pyramidal structures as shown in Fig. 2.9.

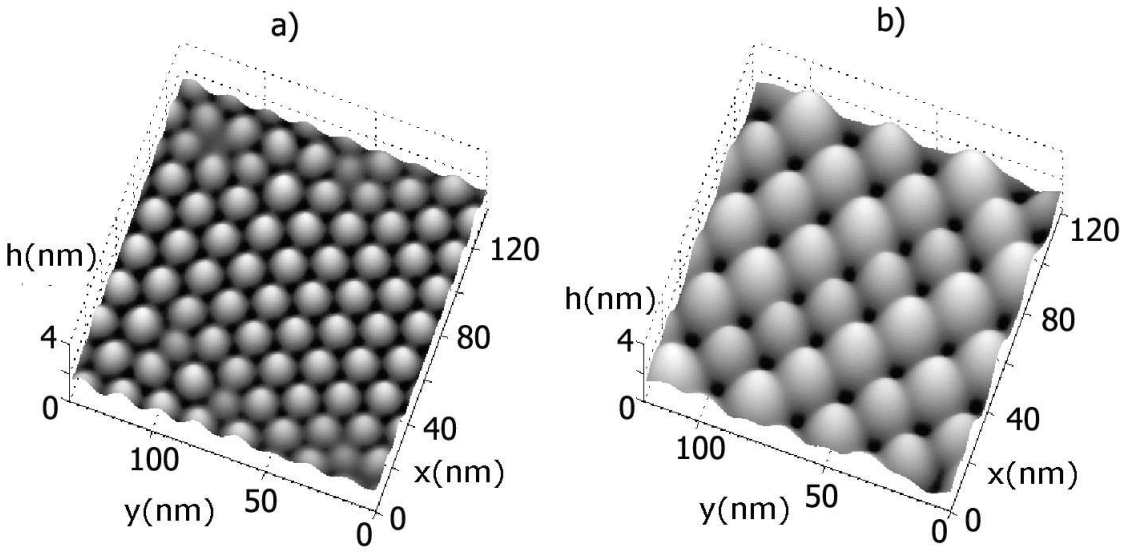

Figure 2.8. Formation of spatially regular arrays of dots: numerical solutions of Eq. (2.16) for [001] surface orientation. a) Stationary hexagonal array of equal-size dots, h_0=1.5 nm, $w = 1.89 \cdot 10^7$ J m^{-3}, $a = 6.6$ J m^{-2} ($w_{01} = .23, \zeta = 1.0$). (b) Stationary square array of equal-size dots, h_0=1.5 nm, $w = 8.2 \cdot 10^5$ J m^{-3}, $a = 11.1$ J m^{-2} ($w_{01} = .01, \zeta = 1.0$). Other parameters are the same as in Figs. 2.4 and 2.5 with $b = 0$.

2.6. Conclusions

We have found that, besides the stress-driven instability, there can be another mechanism for the formation of quantum dots in epitaxially grown thin solid films. By this mechanism, the substrate determines that the film surface initially grows in a specific crystallographic orientation. In the case of a thick film that does not readily "feel" the substrate, this orientation would be forbidden (i.e., thermodynamically unstable), leading to the formation of faceted structures. Wetting interactions between the film and the substrate suppress the long-wave modes of this instability and change its spectrum from the spinodal decomposition type to the Turing type. This spectrum change yields the possibility of the self-organization of stable, spatially regular hexagonal or square arrays

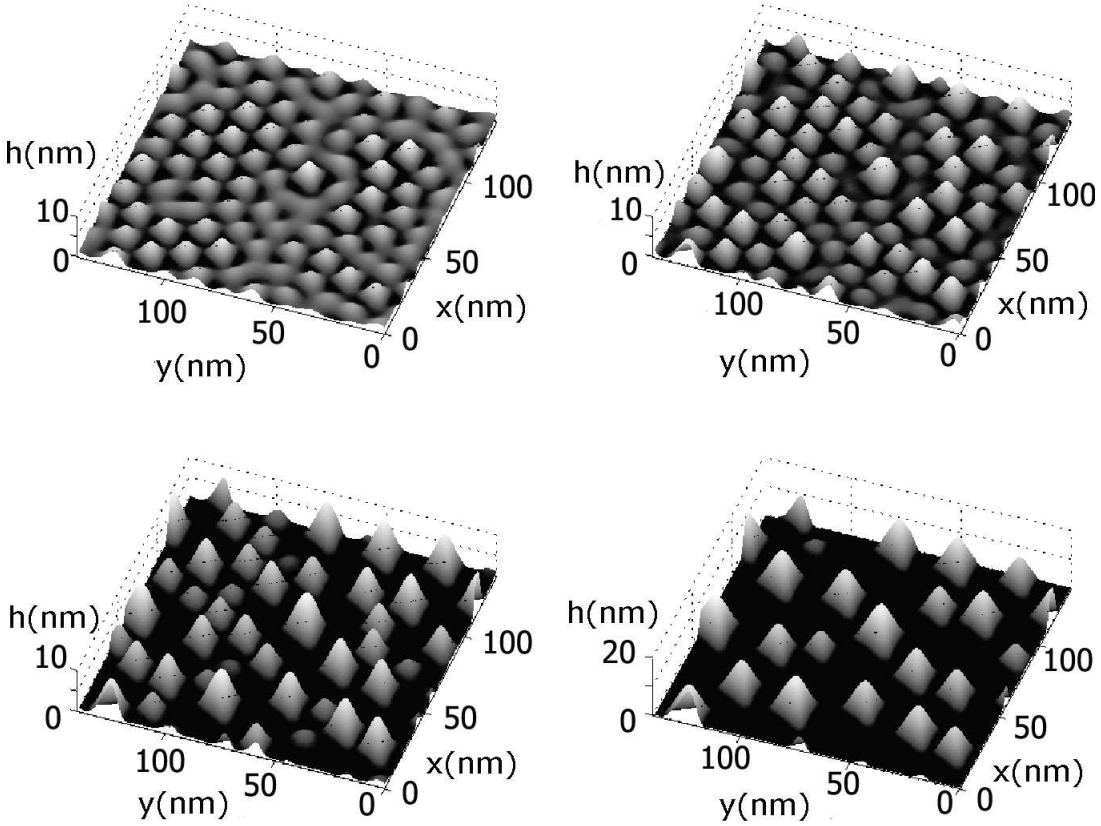

Figure 2.9. Formation of localized dots: numerical solutions of Eq. (2.16) for [111] surface orientation showing different stages of coarsening of initial regular hexagonal array of triangular pyramids for $h_0 = 1.5$ nm, $w = 8.2 \cdot 10^6$ J m^{-2} ($w_{01} = 0.1, \zeta = 1.0$). Other parameters are the same as in Figs. 2.4 and 2.5 except that $b = 0.44$ J m^{-2}.

of equal-sized dots. We have found the parameter regions in which, depending on the type of wetting interactions, one can observe the formation of stable periodic arrays of dots. Note that spatially regular stable arrays of dots caused by wetting interactions exist in a rather narrow range of parameters, bounded by proximity to the instability threshold

and by the stability interval determined by the interaction with the zero mode. Therefore, experimental implementation of the conditions that may lead to the self-assembly of spatially regular arrays of dots can be a challenge for experimentalists.

CHAPTER 3

Self-Assembly of Quantum Dots in a Thin Epitaxial Film Wetting an Elastic Substrate

3.1. Introduction

In the previous chapter, it was shown that, in the presence of a strong surface-energy anisotropy, self-organization of regular QD arrays is possible without epitaxial stress, solely as a result of coupling between wetting interactions and thermodynamic faceting instability. However, as noted in Sec. 2.1, the principle mechanism that leads to the formation of QDs in epitaxial films is associated with epitaxial stress that occurs in the film due to lattice mismatch between the film and the substrate. The elastic energy that accumulates in the film can be lowered by reconstruction of the film surface through surface undulations. This results in the Asaro-Tiller-Grinfeld (ATG) instability [**1**, **2**] leading to the formation of nano-scale surface structures (islands), or QDs [**5**, **6**, **27**].

The theoretical investigation of self-assembly and evolution of quantum dots in thin epitaxial films due to the ATG instability has received a great deal of attention. In [**3**,**7**,**8**], the formation and coarsening of quantum dots caused by the ATG instability mechanism was investigated by numerically solving a nonlinear evolution equation for the film surface shape, and the resulting coarsening kinetics was in agreement with experimental observations [**41**]. Theoretical analysis of stability of a hexagonal array of cones on the surface of an elastically-strained solid was performed in [**42**]. It was shown that elastic interaction

between the cones can lead to array meta-stability. Elastic interactions can also stabilize spatially-regular quantum dot arrays in multi-layer structures [**43**]; however, other stabilization mechanisms are also possible [**44**]. Numerical simulations of self-assembly of regular quantum dot arrays in multilayer structures were performed in [**3**].

Analysis of pattern formation in a thin epitaxial film caused by the interplay between elastic and wetting interactions was performed in [**20**] for the case of a rigid substrate in the long-wave limit; a possibility of the formation of stable, spatially-regular arrays of quantum dots was demonstrated analytically and numerically. A combined effect of elastic stress, surface-energy anisotropy and wetting interactions on the formation of quantum dots in a thin epitaxial film was investigated in [**19**,**45**]. Numerical simulations performed for 1+1 [**45**] and 2+1 interfaces [**19**] showed self-assembly of spatially-periodic arrays of faceted pyramids.

Another important factor that affects the formation of quantum dots in epitaxial films is elastic properties of the substrate. The substrate elasticity results in a non-analytic spectrum of the ATG instability [**5**, **27**] and can substantially affect nonlinear dynamics of quantum dot formation. The effect of the substrate elasticity on self-assembly of quantum dots in the presence of wetting interactions was studied in [**46**]. A non-local, integro-differential equation describing the evolution of the film surface was derived in the long-wave limit, and the formation of a single localized island was investigated (see also [**47**]). This analysis has recently been generalized in [**48**] to include certain nonlinear elastic effects. It was claimed that the combined effect of nonlinear stress and wetting can terminate the coarsening process and lead to the formation of irregular arrays of equal-sized islands. Phase-field numerical simulations of island formation in the presence of

wetting effects and elastic interaction between the film and the substrate were performed in [**49**, **50**].

Despite the large number of theoretical investigations of self-assembly of quantum dots in thin solid films, the question as to the conditions under which the quantum dot coarsening ceases and a spatially-regular array of quantum dots can form still remains open. Specifically, the fact that ordered quantum dot arrays have not been observed in experiments on instability of thin epitaxial films needs to be understood. This problem can be approached by means of weakly nonlinear stability analysis near the ATG instability threshold that would allow one to understand the nature of the bifurcation of a regular pattern from a homogeneous state. Also, it can be shown that wetting interactions between the film and the substrate yield an additional normal stress at the film free surface that can be called a *wetting stress*. This stress originates from the dependence of the wetting potential on the film thickness.

In this chapter, we investigate the formation of quantum dots driven by the ATG instability and wetting interactions between the film and the substrate, accounting for the substrate elasticity and wetting stress. We perform linear and weakly nonlinear analyses to determine the possibility of the formation of spatially-regular quantum dot arrays. We show that, in the case of two-layer and glued-layer wetting potentials, such arrays result from a subcritical bifurcation and are therefore unstable. We also perform numerical simulations of a nonlocal integro-differential equation describing the surface evolution in the long-wave approximation and determine the coarsening kinetics.

3.2. Problem Statement

Consider an epitaxially strained thin solid film that wets a solid, semi-infinite elastic substrate. The film surface, $z = h(\mathbf{x}, t)$, evolves due to surface diffusion, described by [**27**]

$$\frac{\partial h}{\partial t} = \mathcal{D}(1 + |\nabla h|^2)^{1/2} \nabla_s^2 \left[\mathcal{E}(h) - 2\gamma\mathcal{K} + \mathcal{W}(h)\right], \tag{3.1}$$

where z is the coordinate normal to the substrate and $\mathbf{x} = (x, y)$ are the coordinates in the plane parallel to the planar substrate-film interface, ∇_s^2 is the surface Laplace operator defined by Eq. (2.5), $\mathcal{E}(h)$ is part of the surface chemical potential related to the elastic energy in the film which is determined by the solution of the corresponding elastic problem (see below), $\mathcal{W}(h)$ is part of the surface chemical potential due to wetting interactions with the substrate (wetting potential), γ is the surface free energy, assumed to be isotropic, i.e. independent of the surface orientation, $2\mathcal{K} = [(1 + h_x^2)h_{yy} + (1 + h_y^2)h_{xx} - 2h_x h_y h_{xy}]/(1 + |\nabla h|^2)^{3/2}$ is the mean surface curvature, and $\mathcal{D} = D_S S_0 \Omega V_0 / k_B \theta$ (defined in the previous chapter).

As in Chapter 2, we consider two models for the wetting interactions: two-layer and glued-layer. In the two-layer model, the surface energy is an exponentially decaying function of the film thickness described by Eq. (2.10). Since the film surface energy, γ_f, is now assumed to be isotropic, the corresponding wetting potential (2.12) reduces to

$$\mathcal{W}(h) = (d\gamma/dh)/\sqrt{1 + |\nabla h|^2}. \tag{3.2}$$

For the glued-layer wetting model, the wetting potential is given by Eq. (2.13) as in the Chapter 2.

In order to find the elastic energy $\mathcal{E}(h)$, we need to solve the elasticity problem in the film and in the substrate. We choose a coordinate system such that $z = 0$ corresponds to the planar film/substrate interface, $z < 0$ corresponds to the semi-infinite substrate, and $0 < z < h(\mathbf{x}, t)$ corresponds to the film; $\mathbf{x} = (x, y)$ is a position vector in the film plane. We assume that mechanical equilibrium exists in the system at all times; therefore, $\partial_j \sigma_{ij}^{f,s} = 0$, where σ_{ij} is the stress tensor expressed in terms of the strain tensor E_{ij}, ∂_j denotes partial differentiation with respect to the coordinate $j = 1, 2, 3$, corresponding to the coordinates x, y, z, respectively, and the superscripts f and s refer to the film and the substrate, respectively. The stress and strain tensors are related by the Hooke's law [**51**],

$$\sigma_{ij} = 2\mu \left[\left(\frac{\nu}{1+\nu} \right) \delta_{ij} E_{kk} + E_{ij} \right], \quad E_{ij} = \frac{1}{2}(\partial_j u_i + \partial_i u_j), \tag{3.3}$$

where u_i is the ith Cartesian coordinate of the displacement vector, $i = 1, 2, 3$, μ is the elastic shear modulus, ν is the Poisson's ratio, δ_{ij} is the Kronecker's delta, and usual summation over repeated indices is assumed. Thus, the condition of mechanical equilibrium is described by the Navier equation in the film and in the substrate [**51**],

$$(1 - 2\nu^{f,s})\partial_k^2 u_i^{f,s} + \partial_i \partial_k u_k^{f,s} = 0. \tag{3.4}$$

The elastic energy in Eq. (3.1) is $\mathcal{E}(h) = \frac{1}{2}\sigma_{ij} E_{ij}|_{z=h}$.

In the presence of wetting interactions, the boundary conditions that describe the stress balance at the film free surface and at the film-substrate interface require special consideration. In both wetting models, we assume that the wetting potential depends on the film thickness. The latter can change by two mechanisms: (i) accumulation (or redistribution) of material at the free surface and (ii) deformation of the film. If, as a

result of the film deformation, the local displacements of the film free surface and the film-substrate interface in the z-direction are δh_f and δh_s, respectively, then the film thickness changes by $\delta h = \delta h_f - \delta h_s$, causing the film surface energy to change by $(d\gamma/dh)\delta h$. This means that additional stresses in the z-direction, $\mp d\gamma/dh$, act on the film free surface and the film-substrate interface, respectively. The work of these stresses causes this energy change. Similarly, if wetting interactions between the film and the substrate are described by the glued-layer wetting potential given by Eq. (2.13), then the additional stresses acting on the film free surface and the film-substrate interface are $\mp h\, d\mathcal{W}/dh$, respectively. Thus, in the presence of wetting interactions, characterized by an additional wetting energy that depends on the local film thickness, one should include a *wetting stress* acting on the film free surface and on the film-substrate interface. This wetting stress accounts for the change of the film energy due to the variation of the film thickness caused by the film deformation, while the term $\mathcal{W}(h)$ in the surface diffusion equation (3.1) accounts for the change of the film energy when the film thickness changes due to the material redistribution. Note that this consideration is valid only in the long-wave approximation, when wetting interactions can be described by a function that depends on the local film thickness only.

In the following analysis, unless specified otherwise, we consider the two-layer wetting model. Thus, the stress balance boundary conditions at the film free surface and at the film/substrate interface read:

$$\sigma_{ij}^f n_j + \frac{\partial \gamma}{\partial h}\,\delta_{i3} = 0 \quad \text{on } z = h(x,y,t), \tag{3.5}$$

$$\sigma_{ij}^{f} n_j - \sigma_{ij}^{s} n_j + \frac{\partial \gamma}{\partial h} \delta_{i3} = 0 \quad \text{on } z = 0, \tag{3.6}$$

where n_j is the unit normal to the film surface and $\partial\gamma/\partial h$ is the wetting stress.

At the film/substrate interface, continuity of displacement taking into account the lattice mismatch between the film and the substrate holds,

$$u_i^f = u_i^s + \epsilon \begin{bmatrix} x \\ y \\ 0 \end{bmatrix}. \tag{3.7}$$

Here, ϵ is the misfit strain in the film, defined by

$$\epsilon = \frac{a_s - a_f}{a_f}, \tag{3.8}$$

where a_f and a_s are the lattice spacings of the film and the substrate, respectively; $\epsilon > 0$ corresponds to tensile strain and $\epsilon < 0$ to the compressive strain. Finally, we require the strains in the substrate far away from the film to decay to zero,

$$E_{ij}^{s} \to 0 \quad \text{as } z \to -\infty. \tag{3.9}$$

3.3. Steady State Solution

The governing equations in Section 3.2 describe the stress state and surface evolution of an epitaxially strained film. They have a basic state solution corresponding to a completely relaxed, stress-free substrate,

$$\bar{u}_i^s = 0, \quad \bar{\sigma}_{ij}^s = 0, \quad \text{for} \quad i, j = 1, 2, 3, \tag{3.10}$$

and a planar film with spatially uniform stress and strain,

$$\bar{u}_1^f = \epsilon x, \quad \bar{u}_2^f = \epsilon y, \quad \bar{u}_3^f = -\frac{1}{1-\nu_f}\left[2\epsilon\nu_f + \frac{1-2\nu_f}{2\mu_f}\frac{\partial\gamma}{\partial h}\right] z, \tag{3.11}$$

$$\bar{\sigma}_{11}^f = \bar{\sigma}_{22}^f = \frac{1}{1-\nu_f}\left[2\epsilon\mu_f(1+\nu_f) - \nu_f\frac{\partial\gamma}{\partial h}\right], \quad \bar{\sigma}_{33}^f = -\frac{\partial\gamma}{\partial h}. \tag{3.12}$$

Note that even in the absence of epitaxial strain, wetting interactions with the substrate produce *wetting strain* and *wetting stress* in the film:

$$\bar{E}_{33}^w = -\frac{1-2\nu_f}{2\mu_f(1-\nu_f)}\frac{\partial\gamma}{\partial h}, \quad \bar{\sigma}_{11}^w = \bar{\sigma}_{22}^w = -\frac{\nu_f}{1-\nu_f}\frac{\partial\gamma}{\partial h}, \quad \bar{\sigma}_{33}^w = -\frac{\partial\gamma}{\partial h}. \tag{3.13}$$

In the presence of epitaxial strain, wetting interactions modify the strain in the film as well as all components of the stress. It is interesting to note that the presence of wetting stress breaks the symmetry between compressive and tensile epitaxial strains. Indeed, as follows from Eq. (3.11), when the epitaxial strain is compressive ($\epsilon < 0$), the corresponding vertical strain has the same sign as the wetting strain, and the two strains add to increase the total vertical strain. Alternatively, when the epitaxial strain is tensile ($\epsilon > 0$), the signs of the epitaxial and wetting strains in the vertical direction are opposite which decreases the total vertical strain. The total elastic energy stored in the film due to epitaxial and wetting stresses, however, is independent of the sign of ϵ and $\partial\gamma/\partial h$:

$$\mathcal{E}_0 = \frac{1}{2}\bar{\sigma}_{ij}^f\bar{E}_{ij}^f = 2\epsilon^2\mu_f\frac{1+\nu_f}{1-\nu_f} + \frac{1}{2\mu_f}\frac{1-2\nu_f}{1-\nu_f}\left(\frac{\partial\gamma}{\partial h}\right)^2. \tag{3.14}$$

In the next section, we perform the linear stability analysis of this basic state of an epitaxial film in the presence of epitaxial and wetting stresses.

3.4. Linear Stability Analysis

In this section, we study the stability of a planar film in the basic state described by Eqs. (3.10)-(3.12). The film dynamics is governed by equations (3.1),(3.4)-(3.9). We consider infinitesimal perturbations of the planar film, $h = h_0 + \hat{h}e^{\omega t + i\mathbf{k}\cdot\mathbf{x}}$, and the displacement vectors

$$\mathbf{u}^{f,s} = \mathbf{u_0}^{f,s} + \widehat{\mathbf{f}}^{f,s}(z)e^{\omega t + i\mathbf{k}\cdot\mathbf{x}}, \tag{3.15}$$

and linearize the problem (3.1)-(3.9). The solvability condition for the linear problem gives the dispersion relation between the perturbation growth rate ω and the wave vector $\mathbf{k}$. In the long-wave approximation, i.e. for $2\pi/k \gg \bar{h}$, this dispersion relation reads

$$\mathcal{D}^{-1}\omega = -Ak^2 + Bk^3 - Ck^4, \tag{3.16}$$

where $k = |\mathbf{k}|$ and

$$A = \left[1 + \frac{\beta_f}{\mu_f \alpha_f}\gamma'(\bar{h})\right]\gamma''(\bar{h}), \tag{3.17}$$

$$B = 4\frac{\alpha_s}{\alpha_f^2}\mu_0(1+\nu_f)\left\{2\epsilon^2(1+\nu_f)\mu_s - \epsilon\nu_f\left[\gamma'(\bar{h}) + h_0\gamma''(\bar{h})\right]\right\}, \tag{3.18}$$

$$\begin{aligned} C &= \gamma + \frac{2\epsilon h_0}{\alpha_f^3}(1+\nu_f)\left(4\nu_f\gamma'(\bar{h})C_1 + h_0\gamma''(\bar{h})C_2\right) \\ &- \frac{16\epsilon^2 h_0\mu_s}{\alpha_f^3}(1+\nu_f)^2(C_1 - \alpha_f), \end{aligned} \tag{3.19}$$

where

$$\begin{aligned} \alpha_{f,s} &= 2(1-\nu_{f,s}),\ \ \beta_{f,s}=1-2\nu_{f,s},\ \ \mu_0=\mu_f/\mu_s, \\ C_1 &= \alpha_f+\alpha_f\beta_s\mu_0-\alpha_s^2\mu_0^2,\ \ C_2=4\alpha_f+3\alpha_f\beta_s\mu_0-4\alpha_s^2\mu_0^2. \end{aligned} \tag{3.20}$$

The dispersion relation (3.16) is the generalization of the dispersion relation obtained in [**27**], for the case when wetting interactions between the film and the substrate are present. It is valid only if the long-wave approximation holds, $2\pi/k_* \gg h_0$, where k_* is the wave number corresponding to the most rapidly growing mode. In the absence of wetting, for $\gamma'(h_0)=\gamma''(h_0)=0$, $A=0$ and Eq. (3.16) reduces to the long-wave limit of the dispersion relation obtained in [**27**]. (Note that for $\gamma'(h_0)=\gamma''(h_0)=0$ the long-wave expansion (3.16) is valid for $h_0\mu_f\epsilon^2 \ll \gamma$. For typical values of $h_0 = 1$nm, $\mu_s = 10^{12}$ erg/cm^3, $\gamma = 2\cdot 10^3$ erg/cm^2 and $\epsilon = 0.03$ one obtains $h_0\mu_f\epsilon^2/\gamma = 0.05 \ll 1$.)

When wetting interactions between the film and the substrate are present, $\gamma'(h_0) < 0$, $\gamma''(h_0) > 0$, and the dispersion relation contains an additional term, $-Ak^2$, which becomes dominant for small wave-numbers. Had the *wetting stress* not been accounted for, one would have obtained $A=\gamma''(h_0)>0$ which would mean that the wetting interactions always damp long-wave modes. However, this is not always so if the *wetting stress* is taken into account. In this case, the long-wave modes are damped ($A > 0$) only if $|\gamma'(h_0)| < \mu_f\alpha_f/\beta_f \approx 2\mu_f$; otherwise, the long-wave modes are *destabilized* by wetting stress. This de-stabilization is even stronger than that produced by the epitaxial stress; indeed, in this case the growth rate is proportional to k^2, rather than to k^3 in the absence of wetting due to elastic energy accumulated in the film because of the wetting stress.

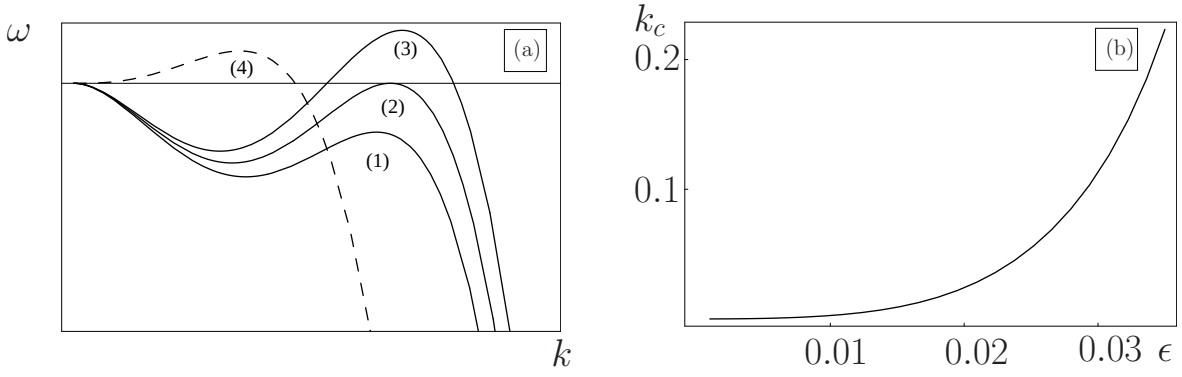

Figure 3.1. (a) Sketch of dispersion curves defined by Eq. (3.16) for (1) $B^2/(4AC) < 1$, (2) $B^2/(4AC) = 1$, (3) $B^2/(4AC) > 1$ and (4) $A = 0$. (b) Critical wave number k_c as a function of the epitaxial strain for the two-layer wetting potential with parameters typical of a Ge on Si system (cgs units): $\mu_f = 10^{12}$, $\mu_0 = 0.8$, $\gamma_f = 2 \cdot 10^3$, $\Delta\gamma = 2 \cdot 10^2$, $\nu_f = 0.198$, $\nu_s = 0.217$.

This effect, however, is probably not relevant to common semiconductor materials, such as Ge or Si. Indeed, taking $\mu_f = 10^{12}$ erg/cm^3, $\gamma_s - \gamma_f \equiv \Delta\gamma = 2 \cdot 10^2$ erg/cm^2, $\delta_w = 1$ nm and $h_0 = 1$ nm, one obtains $\gamma'(h_0) \approx 10^9$ erg/cm^3 (which is in accordance with ab-initio calculations performed in [**31**]) and $\gamma'(h_0) \ll \mu_f$. Thus, in this case $A > 0$, and the long-wave modes are always damped by the wetting interactions. However, for a film made of a material much less stiff than a common semiconductor, this effect may be important.

Typical dispersion curves for the case when wetting interactions damp the long-wave modes are schematically shown in Fig. 3.1(a). The film becomes unstable for $B^2 - 4AC > 0$. One can see that this damping changes the instability spectrum from the long-wave (spinodal decomposition) type to short-wave (Turing) type, thus leading to the possibility of changing the system evolution from Ostwald ripening to the formation of stable spatially periodic patterns. Fig. 3.1(b) shows the wave number $k_c = B/2C$, corresponding to the

most rapidly growing mode, as a function of the lattice mismatch ϵ for typical values of the parameters: $\mu_0 = 0.8,\ \gamma_f = 2 \cdot 10^3,\ \Delta\gamma = 2 \cdot 10^2,\ \nu_f = 0.198,\ \nu_s = 0.217$. One can see that the long wave approximation is valid.

Another interesting effect of wetting stress is associated with the sign of the coefficient B in the dispersion relation (3.16). In the absence of wetting interactions, or if the wetting stress is not taken into account, $B \sim \mu_f \epsilon^2 > 0$ which describes the destabilization effect of the epitaxial stress. The presence of wetting stress can change the sign of this coefficient. Indeed, $\gamma'(h_0) + h_0\gamma''(h_0) = (\Delta\gamma/\delta_w)e^{-h_0/\delta_w}(h_0/\delta_w - 1) \equiv \bar{\gamma}'(h_0) > 0$ for $h_0 > \delta_w$ and $\bar{\gamma}'(h_0) < 0$ for $h_0 < \delta_w$. In the case of a compressive epitaxial strain, $\epsilon < 0$, the coefficient B is positive for $\bar{\gamma}'(h_0) > 2\epsilon\mu_s(1+\nu_f^{-1})$, and in the case of a tensile epitaxial strain, $\epsilon > 0$, the coefficient B is positive for $\bar{\gamma}'(h_0) < 2\epsilon\mu_s(1+\nu_f^{-1})$. This also shows that the presence of the wetting stress *breaks the symmetry* between compressive and tensile epitaxial strains. This effect is more pronounced for *smaller* epitaxial strain.

The stability analysis described above is illustrated in Figs. 3.2–3.6. Fig. 3.2 shows the neutral stability boundaries in the (ϵ, ξ) parameter plane where $\xi = h_0/\delta_w$. One can see that if the epitaxial strain is sufficiently large, then the film is always unstable. However, if the epitaxial strain is small enough, then the film becomes unstable only if its thickness exceeds a critical value, $h_0 > h_c(\epsilon)$. Fig. 3.3 shows that for some intervals of the epitaxial strain and some parameter values there can be *two* critical values of the film thickness, h_c^+ and h_c^-, that bound the *interval* of the film stability. This corresponds to the boxed region in Fig. 3.3(a), enlarged in Fig. 3.3(b). Here, the film is unstable for $h_0 > h_c^+$ and $h_0 < h_c^-$. The film instability for smaller thickness can be explained by the destabilizing effect of

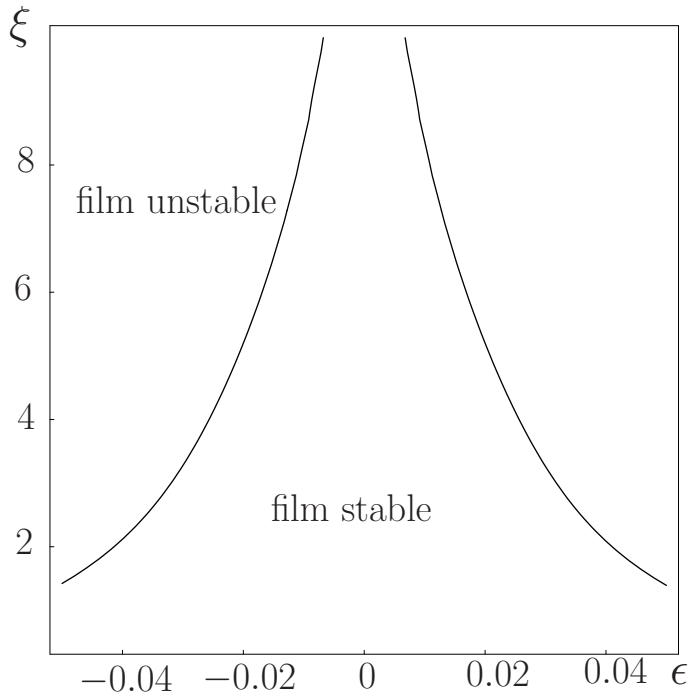

Figure 3.2. Stability regions for a planar epitaxial film with two-layer wetting potential for parameters as in Fig. 3.1.

the wetting stress which is more pronounced for smaller thicknesses due to exponential decay of wetting interactions.

Fig. 3.4 shows how the neutral stability boundaries change as the film stiffness (shear modulus) varies relative to that of the substrate, which is characterized by the parameter μ_0. One can see that the stability region narrows as the film's stiffness increases. Note that the interval of epitaxial strains where the film is stable for $h_c^- < h_0 < h_c^+$ exists only for sufficiently large μ_0.

Fig. 3.5 shows how the neutral stability boundaries change as the wetting strength varies, which is characterized by $\Delta\gamma = \gamma_s - \gamma_f$ in (2.10). One can see that as the wetting interactions become stronger, the film stability region increases.

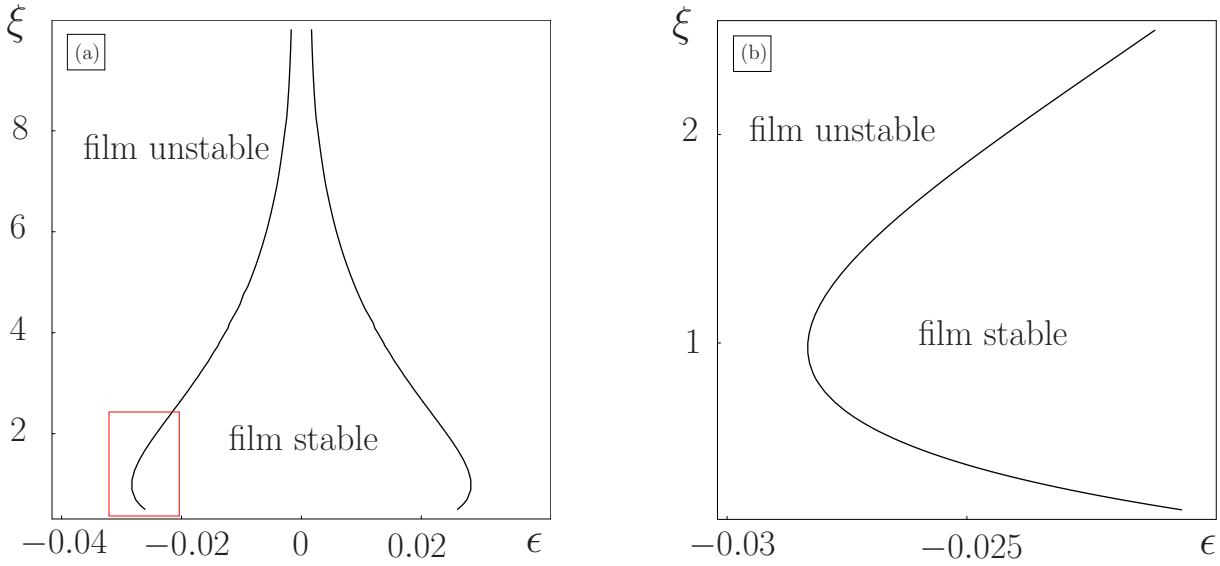

Figure 3.3. (a) Stability regions for a planar epitaxial film with a two-layer wetting potential for $\mu_0 = 10$. See Fig. 3.1 for other parameter values. (b) Zoom of the boxed region in (a).

One can also see from Figs. 3.2–3.5 that for a film with a given thickness there exist two critical values of epitaxial strain (positive and negative for tensile and compressive strains, $\epsilon_c^{\pm}$, respectively) above which the film becomes unstable. Fig. 3.6 shows these critical values of the epitaxial strain as functions of $\Delta\gamma$ and μ_0. In the left figure, one can see $\epsilon_c^{\pm}(\Delta\gamma)$ for $\mu_0 = 10.0$ and different film thickness. In the right figure, one can see $\epsilon_c^{\pm}(\mu_0)$ for $\Delta\gamma = 2 \cdot 10^2$ erg/cm^2 and different thickness of the film. Note that $\epsilon_c^{\pm}$ tend to constant values with the increase of μ_0. Note also that the stability region for $\xi = 1.0$ is larger than those for $\xi = 0.0$ and $\xi = 2.0$. This corresponds to the case shown in Fig.3.3(b).

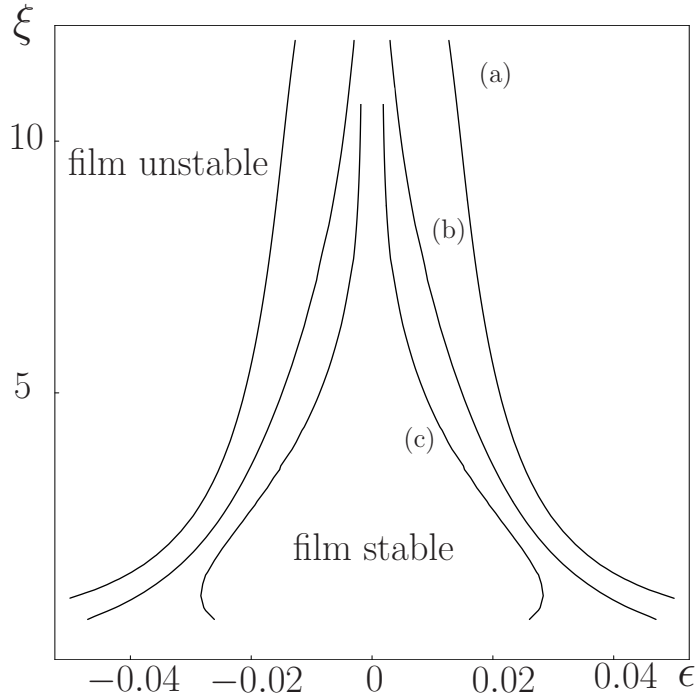

Figure 3.4. Stability regions for a planar epitaxial film with a two-layer wetting potential for: (a) $\mu_0 = 0.01$ (b) $\mu_0 = 0.50$, (c) $\mu_0 = 10$. See Fig. 3.1 for other parameter values.

3.5. Surface Evolution Equation in Long-Wave Approximation

In this section, we derive evolution equation for the shape of the film surface in the long-wave approximation, using the general surface-diffusion equation (3.1). Here we follow closely the derivation presented in [**46**]. We consider the long-wave approximation valid for the case when the wavelength of surface undulations, l, is large relative to the characteristic film thickness h_0.

We introduce a small parameter, $\alpha = h_0/l \ll 1$, rescale the variables: $h \to \alpha l H$, $(x, y) \to l(x', y')$, $z \to \alpha l z'$, $t \to \tau t'$, $u^f_{1,2,3}(x, y, z) \to l U^f_{1,2,3}(x', y', z')$, and consider the expansions $\sigma_{ij} = \sigma^{(0)}_{ij} + \alpha\sigma^{(1)}_{ij} + \alpha^2\sigma^{(2)}_{ij} + \ldots$; $E_{ij} = E^{(0)}_{ij} + \alpha E^{(1)}_{ij} + \alpha^2 E^{(2)}_{ij} + \ldots$; $\mathcal{E} = \mathcal{E}_0 + \alpha\mathcal{E}_1 + \alpha^2\mathcal{E}_2 + \ldots$, where $\mathcal{E}_0 = 2\epsilon^2\mu_f(1+\nu_f)/(1-\nu_f)$. We also use the following scaling

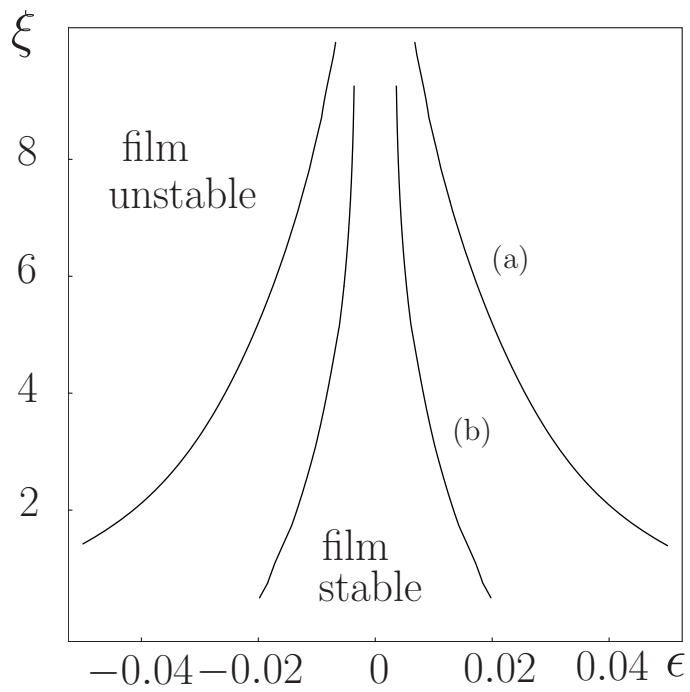

Figure 3.5. Stability regions for a planar epitaxial film with a two-layer wetting potential (cgs units): (a) $\Delta\gamma = 10^2$ and (b) $\Delta\gamma = 1$. See Fig. 3.1 for other parameter values.

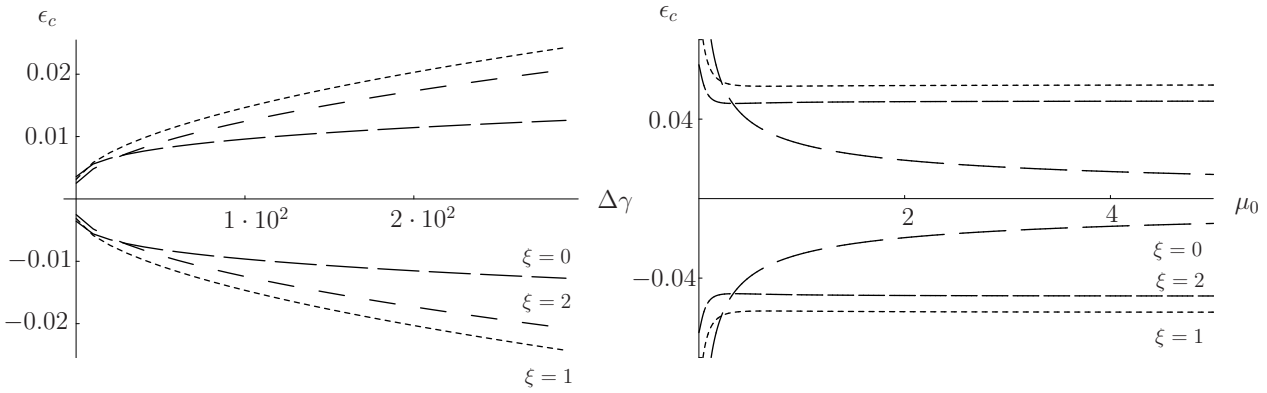

Figure 3.6. Critical values $\epsilon_c^{\pm}$ as functions of $\Delta\gamma$ for $\mu_0 = 10.0$ (left) and μ_0 for $\Delta\gamma = 2 \cdot 10^2$ (right) for different initial film thickness (for a two-layer wetting potential). Other parameter values correspond to those in Fig. 3.1

for the wetting stress: $\partial\gamma/\partial h = \alpha\mu_f\widetilde{\mathcal{W}}(H)$. We choose the time scale $\tau = l^4/(D\gamma_f)$, and the length scale $l = \gamma_f/\mathcal{E}_0$, and obtain from Eq. (3.1), in the order $O(\alpha)$, the following

evolution equation in the long-wave approximation:

$$\frac{\partial H}{\partial t} = \nabla^2[\tilde{\mathcal{E}}_1 - \nabla^2 H + \widetilde{W}]. \tag{3.21}$$

where $\tilde{\mathcal{E}}_1 = \mathcal{E}_1/\mathcal{E}_0$ and $\widetilde{W} = (\mu_f/\mathcal{E}_0)\widetilde{\mathcal{W}}$, and we omit primes in the rescaled coordinates.

We determine $\tilde{\mathcal{E}}_1$ by solving the elasticity problem. First, we find the solution of the elastic problem in the film and the substrate that satisfy the boundary condition (3.5) and (3.6), respectively. We then use the boundary condition (3.7) in order to solve for unknown coefficients of the elasticity problem solution in the film [**46**].

We begin by solving the elasticity problem in the film. Using the long-wave scalings above, we expand the Navier equation (3.4) as

$$\begin{aligned}
&(1-2\nu_f)\left(\frac{\partial^2 U_1^f}{\partial X^2} + \frac{\partial^2 U_1^f}{\partial Y^2} + \frac{1}{\alpha^2}\frac{\partial^2 U_1^f}{\partial Z^2}\right) + \frac{\partial^2 U_1^f}{\partial X^2} + \frac{\partial^2 U_2^f}{\partial X \partial Y} + \frac{1}{\alpha}\frac{\partial^2 U_3^f}{\partial X \partial Z} = 0,\\
&(1-2\nu_f)\left(\frac{\partial^2 U_2^f}{\partial X^2} + \frac{\partial^2 U_2^f}{\partial Y^2} + \frac{1}{\alpha^2}\frac{\partial^2 U_2^f}{\partial Z^2}\right) + \frac{\partial^2 U_1^f}{\partial X \partial Y} + \frac{\partial^2 U_2^f}{\partial Y^2} + \frac{1}{\alpha}\frac{\partial^2 U_3^f}{\partial Y \partial Z} = 0,\\
&(1-2\nu_f)\left(\frac{\partial^2 U_3^f}{\partial X^2} + \frac{\partial^2 U_3^f}{\partial Y^2} + \frac{1}{\alpha^2}\frac{\partial^2 U_3^f}{\partial Z^2}\right) + \frac{1}{\alpha}\frac{\partial^2 U_1^f}{\partial X \partial Z} + \frac{1}{\alpha}\frac{\partial^2 U_2^f}{\partial Y \partial Z} + \frac{1}{\alpha^2}\frac{\partial^2 U_3^f}{\partial Z^2} = 0,
\end{aligned} \tag{3.22}$$

and boundary condition at the film free surface (3.5) as

$$
\begin{aligned}
(3.23)\quad & \frac{2}{1-2\nu_f}\left[\nu_f\left(\frac{\partial U_2^f}{\partial Y}+\frac{1}{\alpha}\frac{\partial U_3^f}{\partial Z}\right)+(1-\nu_f)\frac{\partial U_1^f}{\partial X}\right]\alpha H_X+\left(\frac{\partial U_1^f}{\partial Y}+\frac{\partial U_2^f}{\partial X}\right)\alpha H_Y \\
& \qquad -\frac{1}{\alpha}\frac{\partial U_1^f}{\partial Z}-\frac{\partial U_3^f}{\partial X}=0, \\
& \frac{2}{1-2\nu_f}\left[\nu_f\left(\frac{\partial U_1^f}{\partial X}+\frac{1}{\alpha}\frac{\partial U_3^f}{\partial Z}\right)+(1-\nu_f)\frac{\partial U_2^f}{\partial Y}\right]\alpha H_Y+\left(\frac{\partial U_1^f}{\partial Y}+\frac{\partial U_2^f}{\partial X}\right)\alpha H_X \\
& \qquad -\frac{1}{\alpha}\frac{\partial U_2^f}{\partial Z}-\frac{\partial U_3^f}{\partial Y}=0, \\
& \frac{2}{1-2\nu_f}\left[\nu_f\left(\frac{\partial U_1^f}{\partial X}+\frac{\partial U_2^f}{\partial Y}\right)+\frac{1}{\alpha}(1-\nu_f)\frac{\partial U_3^f}{\partial Z}\right]-\left(\frac{1}{\alpha}\frac{\partial U_1^f}{\partial Z}+\frac{\partial U_3^f}{\partial X}\right)\alpha H_X \\
& \qquad -\left(\frac{1}{\alpha}\frac{\partial U_2^f}{\partial Z}+\frac{\partial U_3^f}{\partial Y}\right)\alpha H_Y+\widetilde{W}(H)=0
\end{aligned}
$$

on $Z=H(X,Y,T)$. We substitute the film displacements expansions,

$$
(3.24)\qquad U_i^f=U_{i0}^f+\alpha U_{i1}^f+\alpha^2 U_{i2}^f+\ldots,
$$

into (3.22) and (3.23), and collect the successive problems in orders of α. At $O(1)$, we have

$$
(3.25)\qquad (1-2\nu_f)\frac{\partial^2 U_{i0}^f}{\partial Z^2}=0
$$

with the boundary conditions

$$
(3.26)\qquad \frac{\partial U_{i0}^f}{\partial Z}=0
$$

for $i = 1, 2, 3$ on $Z = H(X, Y, T)$. Using the steady state solution in Sec. 3.3, we solve Eq. (3.25) and (3.26) and find

$$
\begin{aligned}
U_{10}^f &= \epsilon X, \\
U_{20}^f &= \epsilon Y, \\
U_{30}^f &= 0.
\end{aligned} \tag{3.27}
$$

At $O(\alpha)$, we have

$$
\begin{aligned}
(1-2\nu_f)\frac{\partial^2 U_{11}^f}{\partial Z^2} &= -\frac{\partial^2 U_{30}^f}{\partial X \partial Z}, \\
(1-2\nu_f)\frac{\partial^2 U_{21}^f}{\partial Z^2} &= -\frac{\partial^2 U_{30}^f}{\partial Y \partial Z}, \\
(2-2\nu_f)\frac{\partial^2 U_{31}^f}{\partial Z^2} &= -\frac{\partial^2 U_{10}^f}{\partial X \partial Z} - \frac{\partial^2 U_{20}^f}{\partial Y \partial Z},
\end{aligned} \tag{3.28}
$$

with the boundary conditions

$$
\begin{aligned}
\frac{\partial U_{11}^f}{\partial Z} &= \frac{2\nu_f}{1-2\nu_f}\frac{\partial U_{30}^f}{\partial Z} H_X - \frac{\partial U_{30}^f}{\partial X}, \\
\frac{\partial U_{21}^f}{\partial Z} &= \frac{2\nu_f}{1-2\nu_f}\frac{\partial U_{30}^f}{\partial Z} H_Y - \frac{\partial U_{30}^f}{\partial Y}, \\
\frac{\partial U_{31}^f}{\partial Z} &= \frac{1-2\nu_f}{2(1-\nu_f)}\left(\frac{\partial U_{10}^f}{\partial Z} H_X + \frac{\partial U_{20}^f}{\partial Z} H_Y - \widetilde{W}(H)\right) \\
&\qquad -\frac{\nu_f}{1-\nu_f}\left(\frac{\partial U_{10}^f}{\partial X} + \frac{\partial U_{20}^f}{\partial Y}\right)
\end{aligned} \tag{3.29}
$$

on $Z = H(X, Y, T)$. We use the $O(1)$ solution in (3.28) and (3.29) to obtain

$$
\begin{aligned}
U_{11}^f &= A_{11}(X, Y), \\
U_{21}^f &= A_{21}(X, Y), \\
U_{31}^f &= -\frac{1}{1-\nu_f}\left[2\epsilon\nu_f + \frac{1-2\nu_f}{2}\widetilde{W}(H)\right] Z + A_{31}(X, Y).
\end{aligned} \tag{3.30}
$$

At $O(\alpha^2)$, the displacements in the film satisfy

$$
\begin{aligned}
&(1-2\nu_f)\left(\frac{\partial^2 U_{10}^f}{\partial X^2} + \frac{\partial^2 U_{10}^f}{\partial Y^2} + \frac{\partial^2 U_{12}^f}{\partial Z^2}\right) + \frac{\partial^2 U_{10}^f}{\partial X^2} + \frac{\partial^2 U_{20}^f}{\partial X \partial Y} + \frac{\partial^2 U_{31}^f}{\partial X \partial Z} = 0, \\
&(1-2\nu_f)\left(\frac{\partial^2 U_{20}^f}{\partial X^2} + \frac{\partial^2 U_{20}^f}{\partial Y^2} + \frac{\partial^2 U_{22}^f}{\partial Z^2}\right) + \frac{\partial^2 U_{10}^f}{\partial X \partial Y} + \frac{\partial^2 U_{20}^f}{\partial Y^2} + \frac{\partial^2 U_{31}^f}{\partial Y \partial Z} = 0, \\
&(1-2\nu_f)\left(\frac{\partial^2 U_{30}^f}{\partial X^2} + \frac{\partial^2 U_{30}^f}{\partial Y^2} + \frac{\partial^2 U_{32}^f}{\partial Z^2}\right) + \frac{\partial^2 U_{11}^f}{\partial X \partial Z} + \frac{\partial^2 U_{21}^f}{\partial Y \partial Z} + \frac{\partial^2 U_{32}^f}{\partial Z^2} = 0,
\end{aligned} \tag{3.31}
$$

with the boundary conditions

$$
\begin{aligned}
&\frac{2\nu_f}{1-2\nu_f}\left(\frac{\partial U_{10}^f}{\partial X} + \frac{\partial U_{20}^f}{\partial Y} + \frac{\partial U_{31}^f}{\partial Z}\right) H_X + 2\frac{\partial U_{10}^f}{\partial X} H_X + \left(\frac{\partial U_{10}^f}{\partial Y} + \frac{\partial U_{20}^f}{\partial X}\right) H_Y \\
&\qquad\qquad - \frac{\partial U_{12}^f}{\partial Z} - \frac{\partial U_{31}^f}{\partial X} = 0, \\
&\frac{2\nu_f}{1-2\nu_f}\left(\frac{\partial U_{10}^f}{\partial X} + \frac{\partial U_{20}^f}{\partial Y} + \frac{\partial U_{31}^f}{\partial Z}\right) H_Y + 2\frac{\partial U_{20}^f}{\partial Y} H_Y + \left(\frac{\partial U_{10}^f}{\partial Y} + \frac{\partial U_{20}^f}{\partial X}\right) H_X \\
&\qquad\qquad - \frac{\partial U_{22}^f}{\partial Z} - \frac{\partial U_{31}^f}{\partial Y} = 0, \\
&\frac{2\nu_f}{1-2\nu_f}\left(\frac{\partial U_{11}^f}{\partial X} + \frac{\partial U_{21}^f}{\partial Y} + \frac{\partial U_{32}^f}{\partial Z}\right) + 2\frac{\partial U_{32}^f}{\partial Z} - \left(\frac{\partial U_{11}^f}{\partial Z} + \frac{\partial U_{30}^f}{\partial X}\right) H_X \\
&\qquad\qquad - \left(\frac{\partial U_{21}^f}{\partial Z} + \frac{\partial U_{30}^f}{\partial Y}\right) H_Y = 0
\end{aligned} \tag{3.32}
$$

on $Z = H(X, Y, T)$. Substituting the solutions (3.30) and (3.27) into (3.31) and (3.32), we obtain

$$
\begin{aligned}
U_{12}^f &= \frac{1}{2(1-\nu_f)} \frac{\partial \widetilde{W}}{\partial X} \frac{Z^2}{2} + B_{12}(X,Y)Z + A_{12}(X,Y), \\
U_{22}^f &= \frac{1}{2(1-\nu_f)} \frac{\partial \widetilde{W}}{\partial Y} \frac{Z^2}{2} + B_{22}(X,Y)Z + A_{22}(X,Y), \\
U_{32}^f &= B_{32}(X,Y)Z + A_{32}(X,Y)
\end{aligned} \tag{3.33}
$$

where

$$
\begin{aligned}
B_{12}(X,Y) &= 2\epsilon \frac{1+\nu_f}{1-\nu_f} H_X - \frac{\nu_f}{1-\nu_f} \frac{\partial}{\partial X}(H\widetilde{W}) - \frac{\partial A_{31}}{\partial X}, \\
B_{22}(X,Y) &= 2\epsilon \frac{1+\nu_f}{1-\nu_f} H_Y - \frac{\nu_f}{1-\nu_f} \frac{\partial}{\partial Y}(H\widetilde{W}) - \frac{\partial A_{31}}{\partial Y}, \\
B_{32}(X,Y) &= -\frac{\nu_f}{1-\nu_f} \left(\frac{\partial A_{11}}{\partial X} + \frac{\partial A_{21}}{\partial Y} \right).
\end{aligned} \tag{3.34}
$$

Using the above solutions for the film displacements, we compute the $O(\alpha)$ elastic energy as

$$
\mathcal{E}_1 = \frac{1}{2} \left(\sigma_{ij}^{(0)} E_{ij}^{(1)} + \sigma_{ij}^{(1)} E_{ij}^{(0)} \right) = \frac{2\epsilon \mu_f (1+\nu_f)}{1-\nu_f} \left(\frac{\partial A_{11}}{\partial X} + \frac{\partial A_{21}}{\partial Y} \right). \tag{3.35}
$$

3.5.1. Elastic Response of the Substrate

We determine the unknown functions $A_{11}(X,Y)$ and $A_{21}(X,Y)$ in Eq. (3.35) by solving the elasticity problem in the substrate. We let

$$(x,y,z) = l(X,Y\tilde{Z}), \tag{3.36}$$

$$u_i = lU_i^s, \quad i = 1,2,3,$$

With these scalings, the elasticity equation (3.4) and the far-field condition (3.9) become

$$(1-2\nu)\partial_k^2 U_i^s + \partial_i\partial_k U_k^s = 0, \qquad \text{in} \quad \tilde{Z} < 0, \tag{3.37}$$

$$U_i^s \to 0, \quad \text{as } \tilde{Z} \to \infty. \tag{3.38}$$

We define the Fourier transforms of $\hat{H}(k_X,k_Y)$, $\hat{U}_i^s(k_X,k_Y,\tilde{Z})$, and $\hat{A}_{ij}(X,Y)$,

$$\begin{aligned}
H &= \int_{-\infty}^{\infty}\int_{-\infty}^{\infty} \hat{H} e^{-i(k_X X + k_Y Y)} dk_X dk_Y, \\
U_i^s &= \int_{-\infty}^{\infty}\int_{-\infty}^{\infty} \hat{U}_i^s e^{-i(k_X X + k_Y Y)} dk_X dk_Y, \\
A_{ij} &= \int_{-\infty}^{\infty}\int_{-\infty}^{\infty} \hat{A}_{ij} e^{-i(k_X X + k_Y Y)} dk_X dk_Y, \\
\hat{H} &= \frac{1}{(2\pi)^2}\int_{-\infty}^{\infty}\int_{-\infty}^{\infty} H e^{i(k_X X + k_Y Y)} dX dY, \\
\hat{U}_i^s &= \frac{1}{(2\pi)^2}\int_{-\infty}^{\infty}\int_{-\infty}^{\infty} U_i^s e^{i(k_X X + k_Y Y)} dX dY, \\
\hat{A}_{ij} &= \frac{1}{(2\pi)^2}\int_{-\infty}^{\infty}\int_{-\infty}^{\infty} A_{ij} e^{i(k_X X + k_Y Y)} dk_X dk_Y, \\
k &= \sqrt{k_X^2 + k_Y^2},
\end{aligned}$$

expand the substrate displacements

$$U_i^s = U_{i0}^s + \alpha U_{i1}^s + \alpha^2 U_{i2}^s + \ldots, \tag{3.39}$$

where

$$U_{ij}^s = \int_{-\infty}^{\infty}\int_{-\infty}^{\infty} \hat{U}_{ij}^s e^{-i(k_X X + k_Y Y)} dk_X dk_Y, \tag{3.40}$$

and express Eq. (3.37) as

$$\begin{aligned}
&(1-2\nu)\left(\partial_{\tilde{Z}}^2 - k^2\right)\hat{U}_{1j}^s + ik_X\left(ik_X\hat{U}_{1j}^s + ik_Y\hat{U}_{2j}^s - \partial_{\tilde{Z}}\hat{U}_{3j}^s\right) = 0, \\
&(1-2\nu)\left(\partial_{\tilde{Z}}^2 - k^2\right)\hat{U}_{2j}^s + ik_Y\left(ik_X\hat{U}_{1j}^s + ik_Y\hat{U}_{2j}^s - \partial_{\tilde{Z}}\hat{U}_{3j}^s\right) = 0, \\
&(1-2\nu)\left(\partial_{\tilde{Z}}^2 - k^2\right)\hat{U}_{3j}^s - \partial_{\tilde{Z}}\left(ik_X\hat{U}_{1j}^s + ik_Y\hat{U}_{2j}^s - \partial_{\tilde{Z}}\hat{U}_{3j}^s\right) = 0.
\end{aligned} \tag{3.41}$$

Eq. (3.41) has the solution

$$\begin{bmatrix} \hat{U}_{1j}^s \\ \hat{U}_{2j}^s \\ \hat{U}_{3j}^s \end{bmatrix} = \begin{bmatrix} U_1^{(j)} \\ U_2^{(j)} \\ U_3^{(j)} \end{bmatrix} e^{a\tilde{Z}} + \begin{bmatrix} k_X \\ k_Y \\ k \end{bmatrix} \delta_3^{(j)} \tilde{Z} e^{k\tilde{Z}}, \tag{3.42}$$

where

$$\delta_3^{(j)} = \frac{1}{k(3-4\nu)}\left(k_X U_1^{(j)} + k_Y U_2^{(j)} + ikU_3^{(j)}\right), \tag{3.43}$$

and $U_i^{(j)}$ are constants to determined by the boundary conditions at the film/substrate interface. The misfit condition (3.7) gives

$$
\begin{aligned}
U_{i0}^{s} &= 0, \\
U_{i1}^{f}(Z=0) &= U_{i1}^{s}(\tilde{Z}=0), \\
U_{i2}^{f}(Z=0) &= U_{i2}^{s}(\tilde{Z}=0), \quad i=1,2,3,
\end{aligned} \tag{3.44}
$$

which implies

$$
\begin{aligned}
\hat{A}_{i1} &= U_i^{(1)}, \\
\hat{A}_{i2} &= U_i^{(2)}.
\end{aligned} \tag{3.45}
$$

At $O(\alpha)$, the stress condition (3.6) at the film/substrate interface,

$$
\begin{aligned}
(\sigma_{31}^{f})_1 &= (\sigma_{31}^{s})_1\,, \\
(\sigma_{32}^{f})_1 &= (\sigma_{21}^{s})_2\,, \\
(\sigma_{31}^{f})_3 &= (\sigma_{31}^{s})_3\,,
\end{aligned} \tag{3.46}
$$

gives

$$
-\frac{2\epsilon_0(1+\nu_f)}{1-\nu_f} ik_X \hat{H} + \frac{\nu_f}{1-\nu_f} ik_X (\widetilde{HW})_{\mathbf{k}} = \frac{1}{\mu}\left(kU_1^{(1)} + k_X\delta_3^{(1)} - ik_X U_3^{(1)}\right), \tag{3.47}
$$

$$
-\frac{2\epsilon_0(1+\nu_f)}{1-\nu_f} ik_Y \hat{H} + \frac{\nu_f}{1-\nu_f} ik_Y (\widetilde{HW})_{\mathbf{k}} = \frac{1}{\mu}\left(kU_2^{(1)} + k_Y\delta_3^{(1)} - ik_Y U_3^{(1)}\right), \tag{3.48}
$$

$$
\nu_s\left(-ik_X U_1^{(1)} - ik_Y U_2^{(1)}\right) + (1-\nu_s)\left(aU_3^{(1)} + ik\delta_3^{(1)}\right) = 0, \tag{3.49}
$$

where $\mu = \mu_f/\mu_s$. Solving equations (3.47)-(3.49), we obtain

$$\hat{A}_{11} = \frac{ik_X\mu\left[(H\widetilde{W})_{\mathbf{k}}\nu_f - 2\epsilon H_{\mathbf{k}}(1+\nu_f)\right](1-\nu_s)}{k(1-\nu_f)}, \tag{3.50}$$

$$\hat{A}_{21} = \frac{ik_Y\mu\left[(H\widetilde{W})_{\mathbf{k}}\nu_f - 2\epsilon H_{\mathbf{k}}(1+\nu_f)\right](1-\nu_s)}{k(1-\nu_f)}, \tag{3.51}$$

$$\hat{A}_{31} = \frac{ik_Y\mu\left[(H\widetilde{W})_{\mathbf{k}}\nu_f - 2\epsilon H_{\mathbf{k}}(1+\nu_f)\right](1-2\nu_s)}{2(1-\nu_f)}. \tag{3.52}$$

Finally, we obtain

$$\tilde{\mathcal{E}}_1 = \frac{1}{4\pi^2}\int k\tilde{\mathcal{E}}_{1\mathbf{k}}e^{-i\mathbf{k}\cdot\mathbf{x}}\,d^2\mathbf{k}, \quad \tilde{\mathcal{E}}_{1\mathbf{k}} = E_0\left(-H_{\mathbf{k}} + \frac{1}{2\epsilon}\frac{\nu_f}{1+\nu_f}(H\widetilde{W})_{\mathbf{k}}\right), \tag{3.53}$$

where $H_{\mathbf{k}}$ and $(H\widetilde{W})_{\mathbf{k}}$ are the respective Fourier transforms of H and $H\widetilde{W}$ and

$$E_0 = \frac{2\mu_f(1+\nu_f)(1-\nu_s)}{\mu_s(1-\nu_f)}. \tag{3.54}$$

Eqs. (3.21) and (3.53) are the generalization of the long-wave equation obtained in [**46**] for the presence of wetting stress. However, as shown above, the effect of the wetting stress is negligible for typical semiconductor systems; thus we omit the term $(H\widetilde{W})_{\mathbf{k}}$ in (3.53) in the analysis that follows. After further rescaling, $t \to t/E_0^2$, $\mathbf{x} \to \mathbf{x}/E_0$, Eq. (3.21) has the following form:

$$\frac{\partial H}{\partial t} = \nabla^2[\mathcal{E}_1[H] - \nabla^2 H + W(H)], \tag{3.55}$$

where $W = \widetilde{W}/E_0^2$ and

$$\mathcal{E}_1[H] = \frac{1}{4\pi^2}\int kH_{\mathbf{k}}e^{-i\mathbf{k}\cdot\mathbf{x}}\,d^2\mathbf{k}. \tag{3.56}$$

3.6. Formation of Surface Structures: Weakly Nonlinear Analysis

In this section, we investigate the nonlinear evolution of surface structures near the short-wave instability threshold in order to determine if the formation of a spatially periodic array of dots is possible. We consider $H = H_0 + \widetilde{H}, |\widetilde{H}| \ll H_0$ and expand

$$W(H) = w_0 + w_1\widetilde{H} + w_2\widetilde{H}^2 + w_3\widetilde{H}^3 + \ldots \tag{3.57}$$

Linearizing Eq. (3.55) for $\widetilde{H} \sim e^{\omega t + i\mathbf{k}\cdot\mathbf{x}}$, one obtains

$$\omega = -w_1k^2 + k^3 - k^4. \tag{3.58}$$

The onset of instability corresponds to $w_1 = w_{1c} = 1/4$ and $k = k_c = 1/2$.

Now we consider the weakly nonlinear case corresponding to $w_1 = 1/4 - \varepsilon^2\sigma,\ \varepsilon \ll 1$. First consider quasi-one-dimensional structures (*wires*). We introduce the long scale coordinate $X = \varepsilon x$ and the slow time $T = \varepsilon^2 t$, and consider the expansions

$$\widetilde{H} = \varepsilon(H_1 + \varepsilon H_2 + \ldots), \tag{3.59}$$

$$\mathcal{E}_1 = \mathcal{E}_{10} + \varepsilon\mathcal{E}_{11} + \varepsilon^2\mathcal{E}_{12} + \ldots \tag{3.60}$$

Here,

$$H_1 = \varepsilon\left[A(X,T)e^{ik_cx} + c.c\right], \quad H_2 = \varepsilon^2\left[B(X,T) + A_2(X,T)e^{2ik_cx} + c.c\right], \tag{3.61}$$

where $A(X,T)$ is the complex amplitude of the spatially periodic, unstable mode, and $B(X,T)$ is the real amplitude of the zero mode. The linear operator, $\mathcal{E}_1$, acts on a Fourier mode $A(X,T)e^{ikx}$ as

$$\mathcal{E}_1[A(X,T)e^{ikx}] = \left[\mathcal{E}_{10}(k) + \varepsilon\mathcal{E}_{11}(k,\partial_X) + \varepsilon^2\mathcal{E}_{12}(k,\partial_X) + \ldots\right] A(X,T)e^{ikx}, \tag{3.62}$$

where

$$\mathcal{E}_{10}(k) = -\left|k\right|, \;\; \mathcal{E}_{11}(k,\partial_X) = i\,\mathrm{sgn}(k)\,\partial_X, \;\; \mathcal{E}_{12}(k,\partial_X) = -\mathrm{sgn}(k)\,\partial_{XX}. \tag{3.63}$$

Using these expansions, we obtain successive problems in orders of ε. At $O(\varepsilon^2)$, we find $A_2 = -4w_2A^2$. Finally, the solvability conditions at $O(\varepsilon^3)$ and $O(\varepsilon^4)$ yield the system of coupled amplitude equations:

$$\begin{aligned} A_T &= \frac{1}{4}\sigma A + \frac{1}{2}A_{XX} - \lambda\left|A\right|^2 A + sAB, \\ B_T &= \frac{1}{4}B_{XX} - 4s(|A|^2)_{XX}, \end{aligned} \tag{3.64}$$

where

$$\lambda = \frac{3}{4}w_3 - 2w_2^2, \quad s = -\frac{1}{2}w_2. \tag{3.65}$$

The system of amplitude equations (3.64) has a stable, stationary solution, $A = \left(\frac{\sigma}{4\lambda}\right)^{1/2}, B = 0$, corresponding to spatially periodic patterns if $\lambda > 16s^2$ [**52**], [**20**] i.e. if

$$w_3 > 8w_2^2. \tag{3.66}$$

Condition (3.66) defines a region in the parameter space in which one could observe the formation of stable, periodic array of wires. First consider a *glued-layer* wetting potential defined by Eq. (2.13). Translating (3.66) into physical parameters gives

$$\frac{e^{\xi}[\alpha^3+\xi^3+3\alpha^2(1+\xi)+\alpha(2+3\xi+3\xi^2)]\xi^{1+\alpha}}{12(\alpha+\alpha^2+2\alpha\xi+\xi^2)^2} > \frac{w\gamma_f}{\delta\mathcal{E}_0^2}. \tag{3.67}$$

Combining the instability onset condition $w_1 = 1/4$,

$$\frac{w\gamma_f}{\delta\mathcal{E}_0^2} = \frac{\xi^{\alpha}e^{-\xi}}{4}\left(1+\frac{\alpha}{\xi}\right)^{-1}, \tag{3.68}$$

with (3.67) yields

$$\frac{e^{\xi}[\alpha^3+\xi^3+3\alpha^2(1+\xi)+\alpha(2+3\xi+3\xi^2)]\xi^{1+\alpha}}{12(\alpha+\alpha^2+2\alpha\xi+\xi^2)^2} - \frac{\xi^{\alpha}e^{-\xi}}{4}\left(1+\frac{\alpha}{\xi}\right)^{-1} > 0. \tag{3.69}$$

Eq. (3.69) is satisfied only for $\xi \ll 1$, i.e. for the film thickness which is much smaller than the characteristic wetting length δ_w, which is unrealistic. Thus, one concludes that periodic arrays of wires are unstable in this case.

Now consider a *two-layer* wetting potential defined by Eq. (3.2). We expand (3.2) around the initial film thickness and obtain

$$w_2 = -\frac{w_1}{2}, \quad w_3 = \frac{w_1}{6}. \tag{3.70}$$

Thus, for $w_1 = w_{1c} = 1/4$, we have $\lambda \equiv 0$. In this case, system (3.64) fails to describe periodic pattern with a constant amplitude $A = const$, $B = 0$ since there is no nonlinear saturation; the latter appears in higher orders of ε. Thus we introduce a new slow time scale, $T = \varepsilon^4 t$, and repeat the multiple-scale analysis described above. At $O(\varepsilon^5)$, we

obtain (neglecting spatial modulations of A that decay on the faster time-scale, $\varepsilon^2 t$)

$$A_T = \frac{1}{4}\sigma A - \kappa |A|^4 A, \tag{3.71}$$

where

$$\kappa = \frac{w_1}{4(3+4w_1)} = \frac{1}{64} \tag{3.72}$$

at $w_1 = w_{1c}$. Therefore, for the two-layer wetting model, the amplitude of 1D periodic structures is of $O(\varepsilon^{1/4})$.

We now consider the general case of two-dimensional structures. Due to quadratic nonlinearity, a hexagonal pattern (hexagonal array of dots) will be preferable [**36**, **53**]. We take $\mathbf{X} = \varepsilon \mathbf{x}$, $\tau = \varepsilon t$ and $T = \varepsilon^2 t$, $\varepsilon << 1$, use expansions (3.59), (3.57) and consider

$$H_1 = \sum_{n=1}^{3} A_n(\mathbf{X}, T) e^{i\mathbf{k}_n \cdot \mathbf{x}}, \tag{3.73}$$

$$\begin{aligned} H_2 &= B(\mathbf{X}, T) + \sum_{n=1}^{3} C_n(\mathbf{X}, T) e^{2i\mathbf{k}_n \cdot \mathbf{x}} + D_1(\mathbf{X}, T) e^{i(\mathbf{k}_1 - \mathbf{k}_2)\cdot \mathbf{x}} \\ &+ D_2(\mathbf{X}, T) e^{i(\mathbf{k}_1 - \mathbf{k}_3)\cdot \mathbf{x}} + D_3(\mathbf{X}, T) e^{i(\mathbf{k}_2 - \mathbf{k}_3)\cdot \mathbf{x}} + c.c. + \ldots, \end{aligned} \tag{3.74}$$

where $\mathbf{k}_1 + \mathbf{k}_2 + \mathbf{k}_3 = 0$, $|\mathbf{k}_{1,2,3}| = k_c$. The linear operator $\mathcal{E}_1$ acting on a Fourier harmonic $A(\mathbf{X}, T) e^{i\mathbf{k}\cdot\mathbf{x}}$ is expanded similar to (3.62) as

$$\mathcal{E}_{10}(\mathbf{k}) = -|\mathbf{k}|, \quad \mathcal{E}_{11}(\mathbf{k}, \nabla) = \frac{i}{|\mathbf{k}|}\mathbf{k}\cdot\nabla, \quad \mathcal{E}_{12}(\mathbf{k}, \nabla) = \frac{1}{2|\mathbf{k}|}\left(\nabla^2 - \frac{1}{|\mathbf{k}|^2}(\mathbf{k}\cdot\nabla)^2\right), \tag{3.75}$$

and ∇ acts on the long-scale coordinates $\mathbf{X}$. We substitute these expansions into Eq. (3.21) and obtain the following set of amplitude equations at third and fourth orders of

ε:

$$\frac{\partial A_1}{\partial T} = \frac{1}{4}\sigma A_1 + (\mathbf{k}_1\cdot\nabla)^2 A_1 - \frac{1}{2}w_2 A_2^* A_3^* + 4iw_2\mathbf{k}_1\cdot\nabla(A_2^* A_3^*) - \lambda_1|A_1|^2 A_1 - \lambda_2(|A_2|^2+|A_3|^2)A_1 + sA_1 B, \tag{3.76}$$

$$\frac{\partial B}{\partial T} = \frac{1}{4}\nabla^2 B - 4s\nabla^2(|A_1|^2+|A_2|^2+|A_3|^2), \tag{3.77}$$

where

$$s = -\frac{1}{2}w_2, \quad \lambda_1 = \frac{3}{4}w_3 - 2w_2^2, \quad \lambda_2 = \frac{3}{2}w_3 - \frac{2w_2^2}{2-\sqrt{3}}, \tag{3.78}$$

and equations for A_2 and A_3 are obtained by cyclic permutation of the indices in Eq. (3.76).

The solution of the system (3.76) corresponding to a spatially-periodic, hexagonal array of dots is

$$A = \frac{-w_2/2 - \mathrm{sign}(w_2)\sqrt{w_2^2/4 + \sigma(\lambda_1+2\lambda_2)}}{2(\lambda_1+2\lambda_2)}, \quad B = 0. \tag{3.79}$$

Note that for $w_2 < 0$ it describes the array of dots whereas for $w_2 > 0$ it describes the array of pits. For both the two-layer and glued-layer wetting models $w_2 < 0$. The solution (3.79) is stable for [**52**]

$$\lambda_1 + 2\lambda_2 > 0 \quad \text{and} \quad w_2^2 < \frac{1}{8}(\lambda_1+\lambda_2). \tag{3.80}$$

The first inequality in (3.80) ensures that the hexagonal pattern results from the transcritical bifurcation and the second condition follows from the interaction with the zero mode that effectively renormalizes the Landau constants. It is easy to see that for the

computed values of the Landau coefficients, $\lambda_{1,2}$, the system (3.80) reduces to the first condition, $\lambda_1 + 2\lambda > 0$, or

$$w_3 > \frac{8}{9}\left(5 + \frac{1}{2-\sqrt{3}}\right) w_2^2 \approx 7.76 w_2^2. \tag{3.81}$$

Thus, one can see that the necessary condition for the existence of stable hexagonal arrays of dots is $w_3 > 0$, i.e. $\partial^3 \mathcal{W}/\partial h^3 > 0$. For the *two-layer* wetting potential defined by (3.2), $w_1 = 1/4,\ w_2 = -1/8,\ w_3 = 1/24$ and the condition (3.81) is not satisfied: the hexagonal array of dots results from a subcritical bifurcation in this case and is therefore unstable. For a glued-layer wetting model defined by (2.13) one can check that the condition (3.81) can be satisfied only for $\xi \ll 1$, which is unrealistic. Thus, neither for a two-layer wetting model, nor for a glued-layer one, one can expect the formation of stable, spatially-periodic hexagonal array of dots. This can explain the fact that the formation of such arrays has never been observed in experiments. However, for some other types of wetting potentials the condition (3.81) might be fulfilled and in this case the self-assembly of stable, hexagonally-ordered arrays of QDs would be possible. It is instructive, therefore, to rewrite (3.81) in terms of original physical parameters; it reads:

$$\epsilon^4 \frac{\mu_f^2}{\gamma_f}\left(\frac{\mu_f}{\mu_s}\right)^2 \left(\frac{1+\nu_f}{1-\nu_f}\right)^4 (1-\nu_s)^2 \frac{\partial^3 \mathcal{W}/\partial h^3}{(\partial^2 \mathcal{W}/\partial h^2)^2} > \frac{1}{12}\left(5 + \frac{1}{2-\sqrt{3}}\right) \approx 0.73. \tag{3.82}$$

Also recall that for $\partial^2 \mathcal{W}/\partial h^2 < 0$ one expects the formation of an array of dots whereas for $\partial^2 \mathcal{W}/\partial h^2 > 0$ a hexagonal array of pits will form instead.

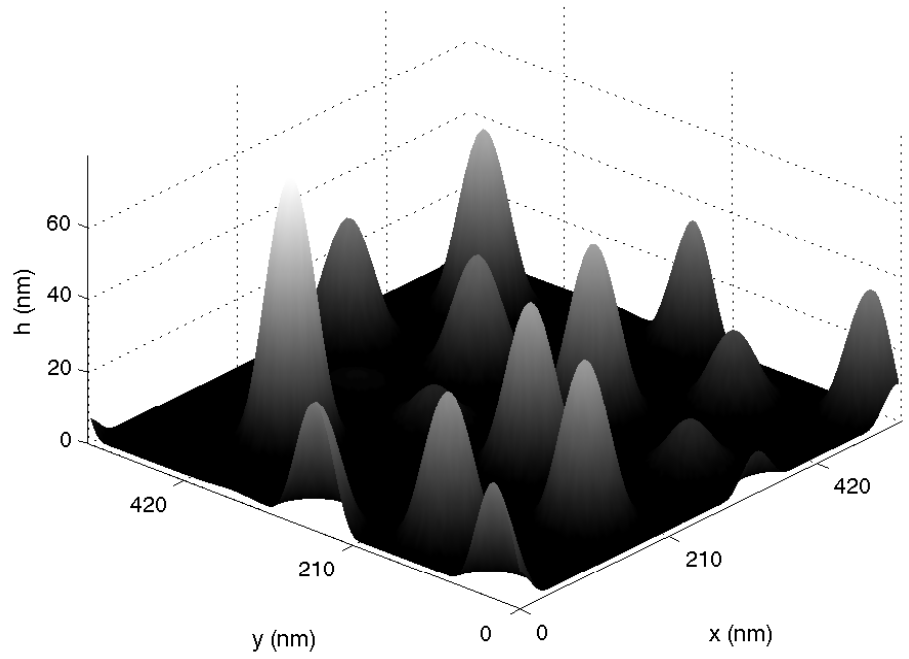

Figure 3.7. Localized QDs: numerical solution of Eq. (3.55) with a glued-layer wetting potential at a particular moment of time for a film with initial thickness $h_0 = 5$ nm, $\delta_w = 2$ nm, $\alpha = 2$, and $\epsilon = 0.025$. Other parameters are (cgs units): $\mu_0 = 0.8,\ w = 10^8,\ \nu_f = 0.198,\ \nu_s = 0.217$.

3.7. Numerical Simulations

We have performed numerical simulations of Eq. (3.55) for the glued-layer wetting potential, $W(H) = \bar{w}H^{-\alpha_w}e^{-H}$, by means of a pseudo-spectral method with the time integration in Fourier space using the Crank-Nicolson scheme for the linear operator and the Adams-Bashforth scheme for the nonlinear operator. The simulations support the main conclusion of the weakly nonlinear analysis: near the instability threshold, the stationary, spatially-periodic structures are unstable as a result of a subcritical bifurcation for $H_0 > 1$. Fig. 3.7 shows the solution of Eq. (3.55) at a particular moment in time in a

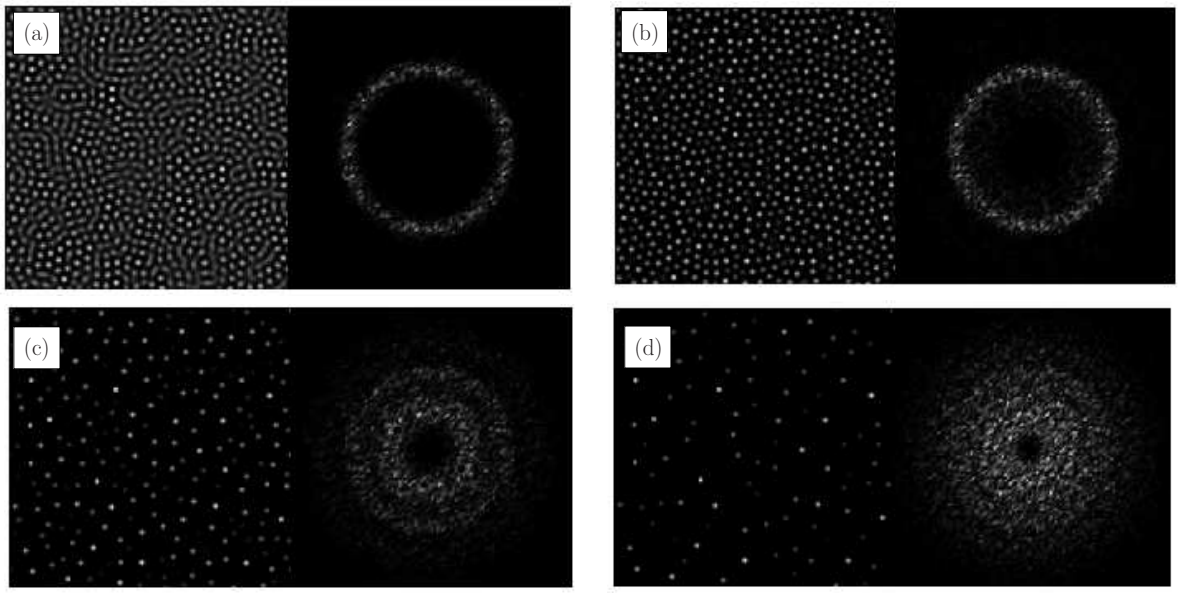

Figure 3.8. Solutions of Eq. (3.55) in real and Fourier spaces for dimensionless times (a) t=200, (b) t=250, (c) t=350, and (d) t=450. The parameters are the same as in Fig. 3.7.

relatively small domain, for small supercriticality. One can see the formation of spatially-localized islands. We have found that this system of islands coarsens in time, with larger islands growing at the expense of the smaller ones.

The formation and evolution of surface structures in a large domain is shown in Fig. 3.8 along with the corresponding Fourier spectra. In Fig. 3.8(a), one can see the formation of the surface structure characterized by the preferred wavelength determined by the linear stability analysis: the Fourier spectrum is a well-defined ring corresponding to the most rapidly growing mode in the narrow interval of unstable modes near k_c. Note that there is no hexagonal ordering in this structure. At later stages (Figs. 3.8b,c,d) the structure exhibits coarsening in that some dots grow in height at the expense of smaller dots and the average distance between the dots increases. Thus the system of spatially-localized

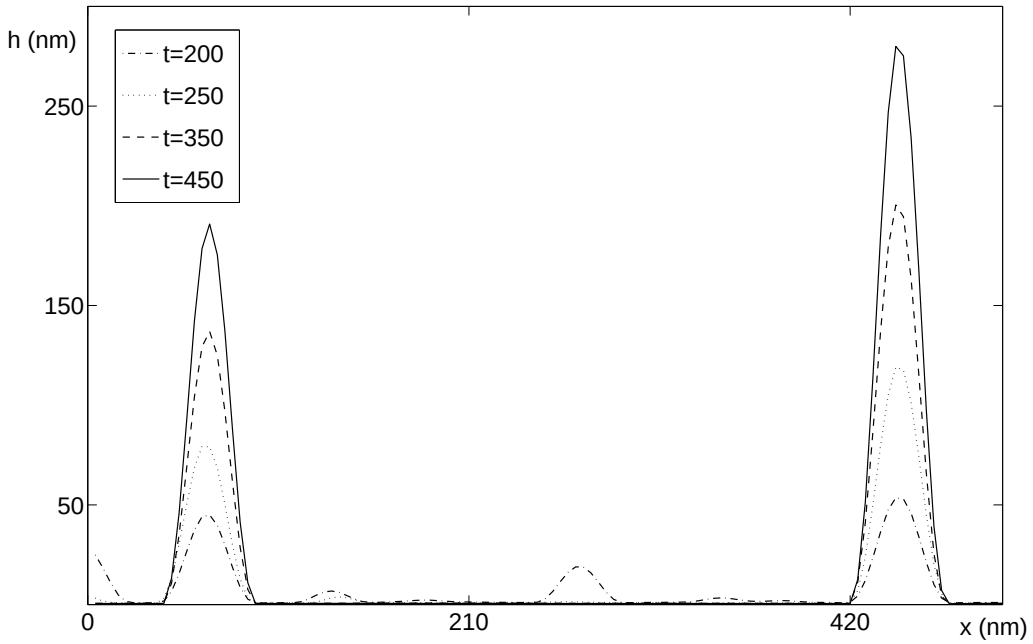

Figure 3.9. Coarsening of QDs: x-cross-section of a numerical solution of Eq. (3.55) at different moments of time. Parameters are the same as in Fig. 3.7.

dots form, with the average distance between the dots much larger than the localization region (dot width). This is also seen in the corresponding Fourier spectra in Figs.8c,d. It is interesting to note that the width of the islands remains almost constant as the structure coarsens. This can be seen in Fig. 3.9. The mass from the shrinking islands is redistributed into the height of the growing islands without contributing to their width.

The coarsening kinetics of QDs can be characterized by different parameters. Fig. 3.10a shows the time dependence of the "root mean square" surface roughness $\langle r \rangle$ suggested in [**48**] defined as $\langle r \rangle = N^{-1}(\sum_{m,n=1,N}[h_{m,n} - h_0]^2)^{1/2}$, where $h_{m,n}$ is the value of h at a discrete point (m, n), $N = 512^2$ is the total number of points, h_0 is the initial film

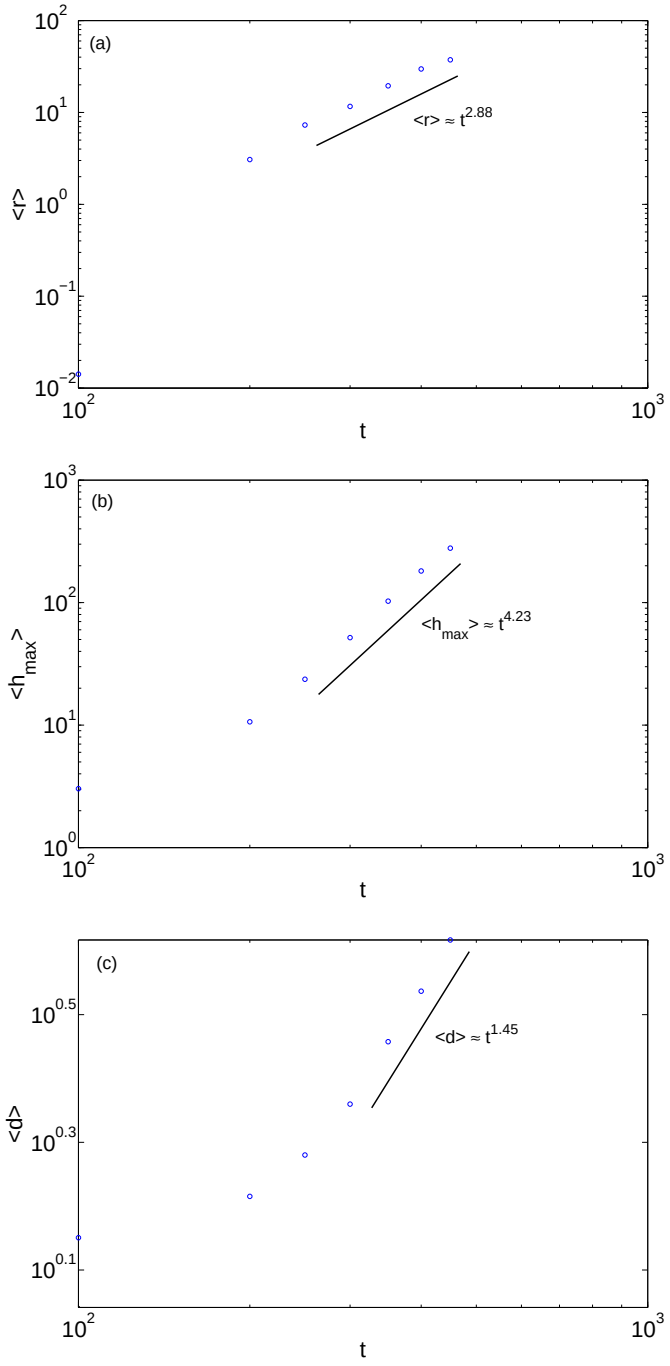

Figure 3.10. Time dependence of (a) root mean square surface roughness, (b) maximum height of surface structures, and (c) average distance between dots.

thickness (equal to the mean value $\langle h \rangle$ due to conservation of mass), and the result is averaged over ten realizations corresponding to ten different random initial data. One can see that $< r > \sim t^{\beta_1}$ where $\beta_1 \approx 2.88$. Fig. 3.10b presents the time dependence of the maximum height of the surface structures, $\langle h_{max} \rangle$ averaged over the realizations. Here, one can see that at the late stages of coarsening $\langle h_{max} \rangle$(t) exhibits the power-law increase, $\langle h_{max} \rangle \sim t^{\beta_2}$, where $\beta_2 \approx 4.23$. Fig. 3.10c shows the average distance between the dots, $\langle d \rangle$, as a function of time. Here, $\langle d \rangle$ is computed as $\langle d \rangle = (N/N_+)^{1/2}$, where N_+ is the number of points for which $h - h_0 > 0$. One can see that $\langle d \rangle \sim t^{\beta_3}$, where $\beta_3 \approx 1.45$. Thus, $\beta_1 \approx 2\beta_3$ and $\beta_2 \approx 3\beta_3$. The origin of the coarsening exponents β_1, β_2 and β_3 and relation between them is yet to be understood.

3.8. Conclusions

We have studied the evolution of the Asaro-Tiller-Grinfeld instability of an epitaxially strained thin solid film on a solid substrate in the case when the film wets the substrate. We have shown that generally, in the presence of wetting interactions, the stress-balance-boundary conditions of the corresponding elasticity problem must include an additional term that describes the *wetting stress* resulting from the dependence of the wetting potential on the film thickness change caused by elastic deformation. We have shown that the wetting stress breaks the symmetry between the tensile and compressive epitaxial strains in that the elastically-stressed state of the planar film and its stability boundaries are different for the different types of epitaxial strain. We have concluded that this is a minor effect for typical semiconductor systems, such as Ge on Si, however, it may be important for hard solid films on relatively soft substrates.

We have derived a non-local, integro-differential equation describing the evolution of the film shape in the long-wave approximation in the general case with the wetting stress. For a typical case when the latter can be neglected (for a typical semiconductor system) we have performed a weakly nonlinear analysis near the instability threshold and have found general conditions on the wetting potential for which self-assembly of spatially-regular arrays of QDs can be observed. We have shown that these conditions are not met in the case of a two-layer and glued-layer wetting potentials and, therefore, spatially-regular QD arrays are unstable in these cases. This can explain the fact that spontaneous formation of spatially regular QD arrays have not been observed in experiments.

We have performed numerical simulations of the derived evolution equation and investigated the formation and evolution of QDs in large domains. We have found that after the structure with the wavelength corresponding to the most rapidly growing mode is formed the system exhibits coarsening, with large islands growing at the expense of the smaller ones. We have also observed that during the coarsening the width of the localized dots remains almost unchanged while the height grows. We have found that the coarsening rate obeys power law, with different characteristics, such as root mean square roughness, maximum dot height and average distance between the dots having different coarsening exponents: $\beta_1 = 2.88$, $\beta_2 = 4.23$ and $\beta_3 = 1.45$, respectively.

CHAPTER 4

Step Flow Growth with Anomalous Diffusion

4.1. Introduction

In Chapters 2 and 3, two instability mechanisms leading to the formation of QDs were studied. These investigations assumed the previous formation of a planar epitaxial film. A typical process of solid film growth is molecular beam epitaxy (MBE) in which atoms are deposited onto a substrate by means of a molecular beam (add). The theory of MBE growth a real crystalline surface has been developed extensively. In the seminal paper by Burton, Cabrera, and Frank (BCF), a quantitative model for the growth of a stepped crystal surface was proposed [**54**]. An infinite surface formed by high-symmetry terraces of length l separated by monoatomic steps was considered. The step flow resulted from adatom deposition onto the surface followed by their diffusion and subsequent incorporation into the step. Adatoms not captured by a step desorbed back into the gas phase after a characteristic time τ. A schematic of this step-flow mechanism is shown in Fig 4.1 where F is the rate of adatom deposition. In the quasistationary approximation, analytical expressions for the adatom density between two terraces and the propagation of an individual step edge perpendicular to the surface were determined. The adatom density was found to vary as hyperbolic cosine with the maximum concentration at the center of the terrace. The step flow velocity as a function of the terrace length was determined to increase monotonically and saturate in the limit of an infinite terrace. One important

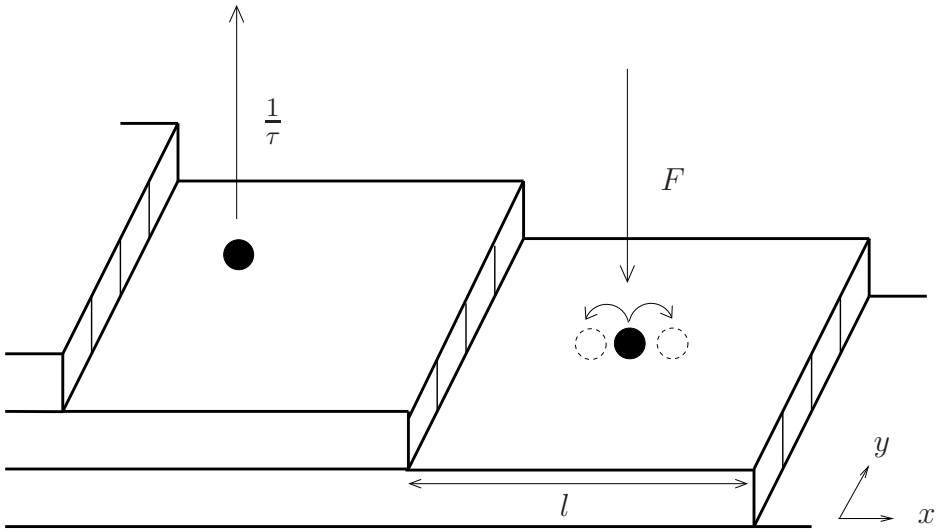

Figure 4.1. Two-dimensional schematic of the growth and evaporation of a stepped surface.

feature of this model is that adatoms that reach a step are assumed to attach to it with equal probability, regardless of whether the adatom approaches the step edge from the upper or lower terrace.

In the BCF model, the mechanism that governs the movement of adatoms on the surface is normal diffusion, where the transport is a result of independent random nearest-neighbor jumps that follows Gaussian statistics characterized by the time dependence, $< (\Delta \mathbf{r})^2 > \sim t$, where $< (\Delta \mathbf{r})^2 >$ is the mean-squared displacement of a randomly walking adatom. However, in many systems, the particle transport deviates from this linear dependence and instead obeys the power law, $< (\Delta \mathbf{r})^2 > \sim t^{\alpha}$, where $\alpha \neq 1$. This is known as anomalous diffusion [**55**]. When $0 < \alpha < 1$, the diffusion is slower than normal and called "subdiffusion;" when $1 < \alpha < 2$, the diffusion is faster and called "superdiffusion." Subdiffusion tends to arise in systems where there are spatial or temporal restraints that force the particle to take long rests between jumps, with specific waiting time probability

distribution. Such is the case for the diffusion in gels and porous media in which the corresponding random walk is accompanied by a specific distribution of resting/binding times between periods of free diffusive motion [**56**]. Superdiffusion typically arises in systems where the particle makes frequent long jumps and occurs in surface diffusion and turbulent or chaotic processes [**57**]. A special case of superdiffusive processes are Lévy flights which have diverging mean squared displacements [**55**].

Due to the fractional power law relation described above, anomalous diffusion processes can be described by non-local integro-differential equations. Lévy flights are governed by the following equation

$$\frac{\partial u}{\partial t} = \frac{\partial^\beta u}{\partial |x|^\beta}, \tag{4.1}$$

where the fractional derivative operator is defined through its Fourier transform as

$$\mathcal{F}[\partial^\beta u/\partial |x|^\beta](k) = -|k|^\beta \mathcal{F}[u](k). \tag{4.2}$$

In this chapter, we consider step-flow growth of a vicinal crystal surface in the case when adatom transport along the terraces between the steps is governed by Lévy flights. We develop the analog of the BCF theory for the case of Lévy flights and obtain the step-flow velocity as an eigenvalue of the corresponding superdiffusion problem described by a fractional partial differential equation. The resulting crystal surface growth rate is found as a function of the terrace length and the anomalous diffusion exponent β.

4.2. Problem Formulation

We consider the growth of a stepped crystal surface by molecular beam epitaxy (MBE) in the case when the diffusion of adatoms on the surface is anomalous, in particular, superdiffusive (Lévy flights). We assume that the surface consists of high-symmetry orientation terraces of equal width l separated from each other by parallel steps with monoatomic height. A molecular beam deposits adatoms onto the surface at a rate F, and the adatoms then perform Lévy flights along the terraces. After a characteristic time τ, some adatoms desorb back into the gas phase while others eventually reach a step. The step attachment kinetics is infinitely fast so that the adatom concentration in the neighborhood of each step attains its equilibrium value ρ_0; each step therefore acts as a perfect sink. We let $\rho(x,t)$ be the density of adatoms deposited between two steps, sufficiently low to avoid the possible nucleation of new terraces between adjacent steps. The adatom density along one terrace is described by the following boundary value problem:

$$\begin{aligned} \frac{\partial \rho}{\partial t} - \mathcal{D}_s \frac{\partial^\beta \rho}{\partial |x|^\beta} + \frac{1}{\tau}\rho &= F - M \sum_{n=-\infty}^{\infty} \delta(x - n\,l - vt), \\ \rho(n\,l + vt) &= \rho_0, \end{aligned} \tag{4.3}$$

where x is the direction perpendicular to the steps, $\mathcal{D}_s$ is the (anomalous) surface diffusion coefficient, M is the intensity of the step sinks, v is the step velocity, and $\partial^\beta \rho / \partial |x|^\beta$ is the fractional diffusion term defined by (4.2) where $(1 < \beta < 2)$ where $\beta = 2$ corresponds to normal diffusion. The model is similar to the standard BCF formulation with the distinction that the normal diffusion term is replaced by an anomalous one. Physically this accounts for the nonzero probability that a diffusing adatom makes a long jump that

prevents it from reaching and attaching to the nearest step. As a result, the propagation of an individual step depends globally on the adatom concentration on the terraces between the other steps. The steps are represented in Eq. (4.4) as an infinite series of delta functions separated by distance l corresponding to moving sinks.

We introduce the spatial and temporal scales, $\hat{x} = (\mathcal{D}_s\tau)^{-1/\beta}x$, $\hat{t} = t/\tau$ and nondimensionalize Eq. (4.3). Dropping the hats, we define $u(x,t) = \rho(x,t) - \tau F$, $u_0 = \tau F - \rho_0$, and let $u \to u + u_0$. Eq. (4.3) then becomes

$$
\begin{aligned}
-\frac{\partial u}{\partial t} + \frac{\partial^\beta u}{\partial |x|^\beta} - u &= -u_0 + J\sum_{n=-\infty}^{\infty}\delta(x - nL - Vt), \\
u(nL + Vt) &= 0,
\end{aligned}
\tag{4.4}
$$

where J and V are the dimensionless sink intensity and step velocity, respectively. In the moving frame, $x \to x + Vt$, the problem (4.4) reads

$$
\begin{aligned}
\frac{\partial^\beta u}{\partial |x|^\beta} + V\frac{\partial u}{\partial x} - u &= -u_0 + J\sum_{n=-\infty}^{\infty}\delta(x - nL), \\
u(nL) &= 0.
\end{aligned}
\tag{4.5}
$$

The step speed V is determined by the total adatom flux into the sink, $V = -[j]$, where

$$
j = \frac{1}{2\pi}\int \frac{|k|^\beta}{ik}\hat{u}(k)\, e^{ikx}dk \tag{4.6}
$$

is the flux governed by Lévy flight,

$$
\hat{u}(k) = \int_{-\infty}^{\infty} u(x)e^{-ikx}dx \tag{4.7}
$$

is the Fourier transform of $u(x)$ and $[j] = j_+ - j_-$ denotes the jump across the step. Integrating Eq. (4.6) across one step yields $V = J$.

4.3. Quasistationary Approximation

We begin by solving Eq. (4.5) in the quasistationary approximation, assuming that the diffusion of atoms along the terrace is much faster than the step motion. Thus, we neglect the convective term in Eq. (4.5). We transform Eq. (4.5) into Fourier space using (4.7), solve for $\hat{u}(k)$, and invert back with

$$u(x) = \frac{1}{2\pi} \int_{-\infty}^{\infty} u(k) e^{ikx}\, dk \tag{4.8}$$

to obtain the adatom density

$$u(x) = u_0 - \frac{J}{2\pi} \sum_{n=-\infty}^{\infty} \int_{-\infty}^{\infty} \frac{e^{ik(x-nL)}}{|k|^\beta + 1}\, dk. \tag{4.9}$$

The sink intensity is found from the condition $u(0) = 0$ as

$$J = 2\pi u_0 \left(\sum_{n=-\infty}^{\infty} \int_{-\infty}^{\infty} \frac{e^{-iknL}}{|k|^\beta + 1}\, dk \right)^{-1}. \tag{4.10}$$

Eq. (4.10) gives the expression for the step velocity $V = J$. The integrals in Eqs. (4.9) and (4.10) can be evaluated using the Poisson summation formula which states that the sum of a function $u(x)$ over all integers is equal to the equivalent summation over its continuous Fourier transform $\hat{u}(k)$ defined in Eq. (4.7); in our case, we have

$$\sum_{n=-\infty}^{\infty} e^{-iknL} = \frac{2\pi}{L} \sum_{n=-\infty}^{\infty} \delta\left(k - \frac{2n\pi}{L}\right). \tag{4.11}$$

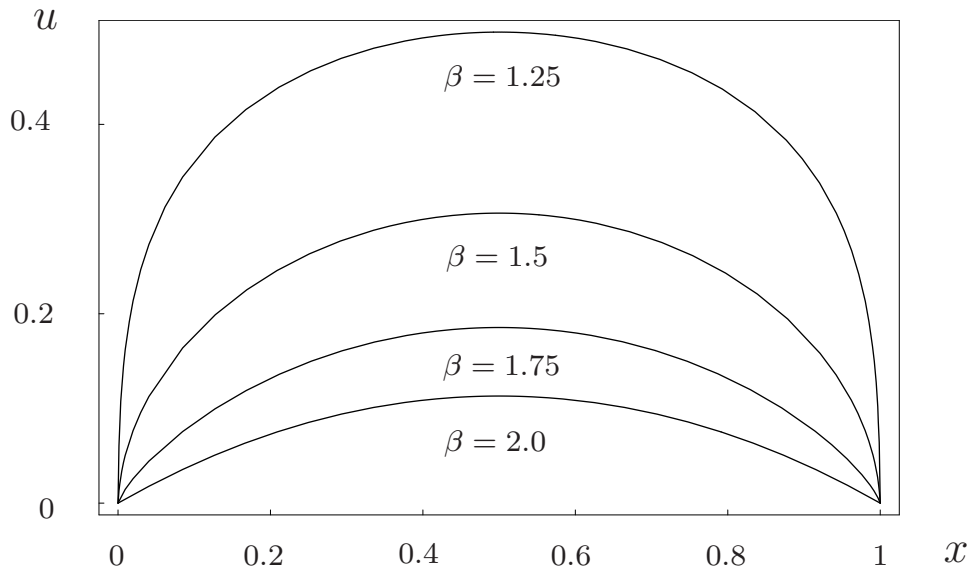

Figure 4.2. Variation in the adatom density u between two steps for anomalous diffusion exponents $\beta = 1.25$, $\beta = 1.5$, and $\beta = 1.75$, and for normal diffusion exponent $\beta = 2.0$.

Thus, the solutions for the adatom density and step flow velocity, (4.9) and (4.10), reduce to

$$u(x) = u_0 - \frac{J}{L}\left(1 + 2\sum_{n=1}^{\infty}\frac{\cos(\lambda_n x)}{\lambda_n^{\beta}+1}\right), \tag{4.12}$$

$$J = V = u_0 L\left(1 + 2\sum_{n=1}^{\infty}\frac{1}{\lambda_n^{\beta}+1}\right)^{-1}, \tag{4.13}$$

where $\lambda_n = 2n\pi/L$. Fig. 4.2 shows the adatom density given by Eq. (4.12) for varying Lévy exponents. One can see that smaller values of β result in more concentrated density distributions with stronger concavity. The adatom density profiles suggest that, for decreasing β, fewer adatoms attach to a step edge. This is reasonable since adatoms that jump further have lower step attachment probabilities than those that perform only nearest neighbor walks. More adatoms thus accumulate near the center of the terrace,

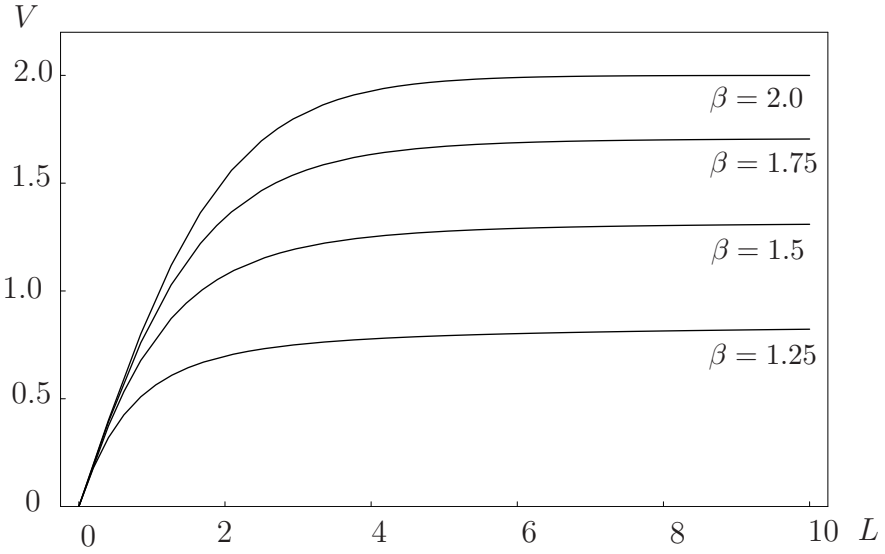

Figure 4.3. Variation of the step velocity V with the terrace length L for anomalous diffusion exponents $\beta = 1.25$, $\beta = 1.5$, and $\beta = 1.75$, and for normal diffusion exponent $\beta = 2.0$.

providing a possible explanation for the wider and flatter maximums in the density profiles. Since fewer adatoms attach to a step, the propagation of a step must decrease for smaller β. Fig. 4.3 shows the step flow as a function of the terrace length L for different values of the diffusion exponent. One can see that the step flow decreases for smaller diffusion exponents and that it saturates in the limit of an infinite terrace. To determine the saturation velocity, we define $\epsilon \equiv 1/L, \epsilon \ll 1$, and rewrite Eq. (4.13) as

$$V_{sat} = u_0 \left(\epsilon + 2 \sum_{n=1}^{\infty} \frac{\epsilon}{(2n\pi\epsilon)^{\beta} + 1} \right)^{-1}. \tag{4.14}$$

Using the substitution $x = 2\,n\,\pi\epsilon$ we have, in the limit as $\epsilon \to 0$,

$$V_{sat} = \pi u_0 \left(\int_0^{\infty} \frac{x^{\mu}}{x(1+x)} dx \right)^{-1}, \tag{4.15}$$

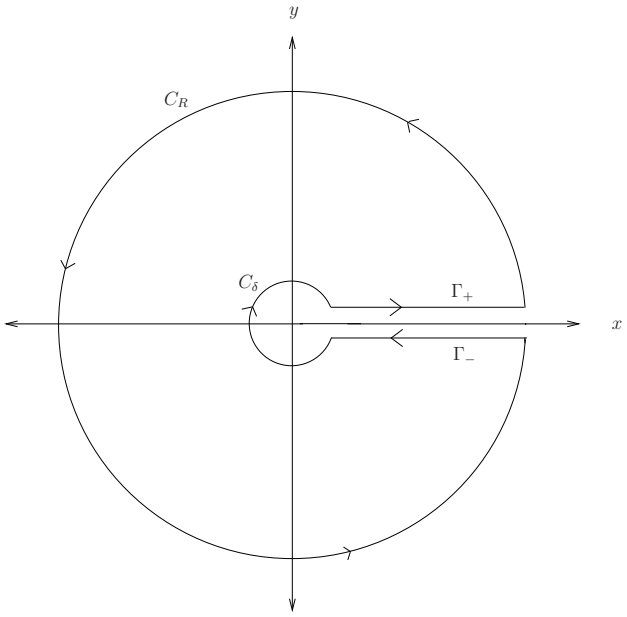

Figure 4.4. Sketch of integration contour C in Eq. (4.16)

where $\mu = 1/\beta$. The integral in Eq. (4.15) can be evaluated exactly by considering

$$I = \int_C \frac{z^\mu}{z(1+z)} dz \tag{4.16}$$

in the complex plane where C is the closed contour shown in Fig. 4.4 consisting of the circle C_R of radius R centered at the origin, the segment $\Gamma_- : R \geq x \geq \delta$, $\delta << 1$, of the x-axis, the circle C_δ of radius δ centered at the origin and the segment $\Gamma_+ : \delta \leq x \leq R$ of the x-axis. The integrals on C_R and C_δ go to zero as $R \to \infty$ and $\epsilon \to 0$, respectively. We then have

$$(1 - e^{2\pi i \mu}) \int_0^\infty \frac{x^\mu}{x(1+x)} dx = 2\pi i (-1)^{\mu - 1}, \tag{4.17}$$

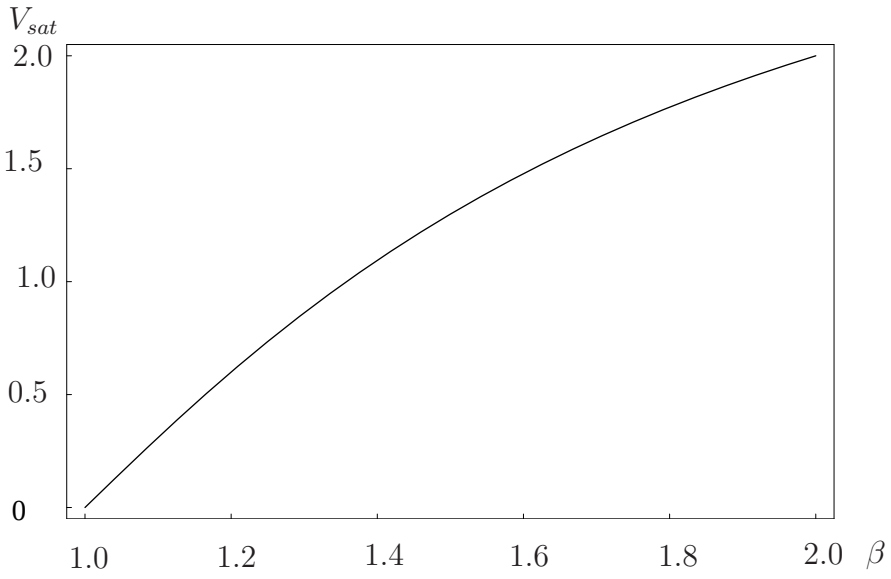

Figure 4.5. Saturation velocity V_{sat} as a function of the diffusion exponent β.

where the right hand side is the contribution from the residue at $z = -1$. Thus we obtain

$$V_{sat} = \beta u_0 \sin\left(\frac{\pi}{\beta}\right) \tag{4.18}$$

as shown in Fig. 4.5.

4.4. Full Problem

We now determine the step flow velocity without making the quasistationary approximation. Proceeding in a similar manner as in Section 4.3, we transform Eq. (4.5) into Fourier space, solve for $\hat{u}(k)$, and invert back to real space. After applying the boundary

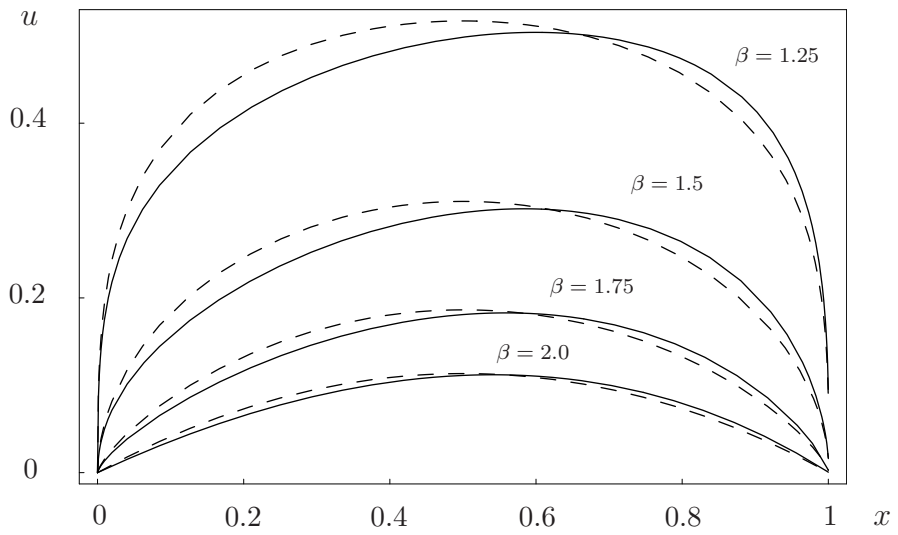

Figure 4.6. Adatom density u between two steps for the quasistationary approximation and the full problem for anomalous diffusion exponents $\beta = 1.25$, $\beta = 1.5$, and $\beta = 1.75$, and for normal diffusion exponent $\beta = 2.0$

.

conditions, we find the adatom density

$$u(x) = u_0 - \frac{J}{2\pi} \sum_{n=-\infty}^{\infty} \int_{-\infty}^{\infty} \frac{e^{ik(x-nL)}}{|k|^\beta + 1 - ikV}\, dk, \tag{4.19}$$

$$J = V = u_0 L \left\{ \sum_{n=-\infty}^{\infty} \int_{-\infty}^{\infty} \frac{e^{-iknL}}{|k|^\beta + 1 - ikV}\, dk \right\}^{-1}. \tag{4.20}$$

As in the quasistationary case, Eqs. (4.19) and (4.20) can be simplified using the Poisson summation formula (4.11). Thus, we have

$$u(x) = u_0 - \frac{J}{L} \left[1 + 2 \sum_{n=1}^{\infty} \frac{(1+\lambda_n^\beta)\cos(\lambda_n x) + \lambda_n V \sin(\lambda_n x)}{(1+\lambda_n^\beta)^2 + (\lambda_n V)^2} \right], \tag{4.21}$$

$$J = V = u_0 L \left[1 + 2 \sum_{n=1}^{\infty} \frac{1+\lambda_n^\beta}{(1+\lambda_n^\beta)^2 + (\lambda_n V)^2} \right]^{-1}. \tag{4.22}$$

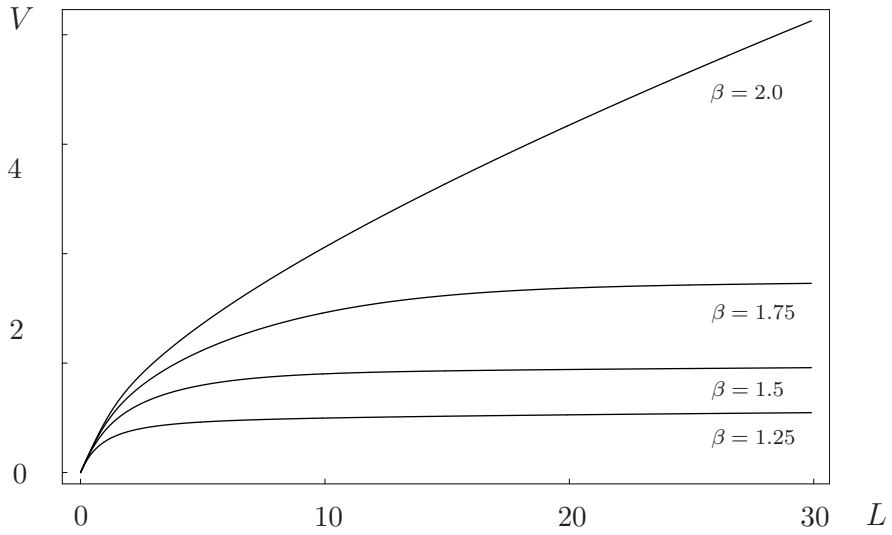

Figure 4.7. Variation of the step velocity V with the terrace length L for anomalous diffusion exponents $\beta = 1.25$, $\beta = 1.5$, and $\beta = 1.75$, and for normal diffusion exponent $\beta = 2.0$.

Note that Eq. (4.22) is a transcendental equation for the step flow velocity V.

Fig. (4.6) shows the adatom densities given by Eq. (4.21) together with those from the quasistationary approximation (4.12) for varying diffusion exponents. The dashed and solid curves correspond to the quasistationary and full solutions, respectively. As in the quasistationary approximation, one can see that smaller values of the diffusion exponent β result in more concentrated atom density profiles. However in this case, the atom density is no longer symmetric about the center of the terrace. The distribution is instead skewed towards the right as compared with the quasistationary approximation with lower and higher densities near the respective left and right sides of the terrace. As the step propagates it captures atoms in its vicinity and incorporates them into the step; thus the concentration of atoms on the terrace decreases in this region. The atoms move

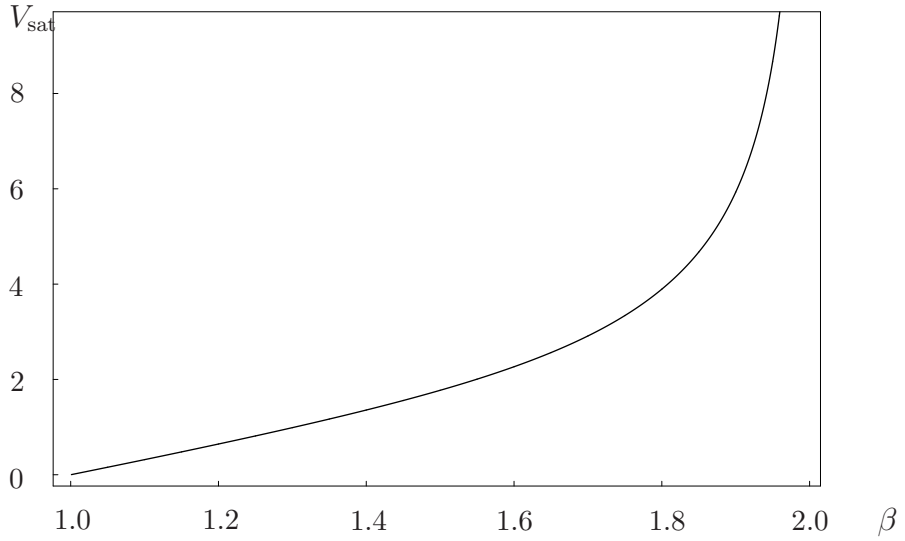

Figure 4.8. Saturation velocity V_{sat} as a function of the diffusion exponent β.

away from the advancing step which causes the density on the right side of the terrace to increase.

Since the adatom density distribution is greater for Lévy flights than for normal diffusion, the corresponding step flow velocity is slower. Fig. 4.7 shows the step flow velocity as a function of terrace length for different values of β. One can see that the step velocity saturates for $1 < \beta < 2$ and becomes infinite as $\beta \to 2$. We determine the saturation velocity by introducing $\epsilon \equiv 1/L$, making the substitution $x = 2\,n\,\pi\epsilon$ and letting $\epsilon \to 0$. Eq. (4.22) then becomes

$$V_{sat} = \pi u_0 \left[\int_0^\infty \frac{1 + x^\beta}{(1 + x^\beta)^2 + (x V_{sat})^2}\, d\,x \right]^{-1}. \tag{4.23}$$

Eq. (4.23) is a transcendental equation for V_{sat} which we solve numerically. The solution is shown in Fig. 4.8 as a function of β.

4.5. Conclusions

We have studied the growth of a stepped crystalline surface by molecular beam epitaxy in the case when the diffusion of adatoms on the surface is governed by Lévy flights. For the quasistationary approximation and full problems, we have determined analytical solutions for both the density of adatoms on a terrace and the step flow velocity. In both cases, we have found that step flow governed by Lévy flights is slower than that of normal diffusion due to fewer adatoms reaching the step.

We have also determined the step flow velocity asymptotically for large terrace length. In the quasistationary approximation, we have found that the step flow saturates for all values of the anomalous diffusion exponent. However, for the full problem, we have found that the saturation velocity tends to infinity in the limit of normal diffusion.

CHAPTER 5

Conclusions

In this thesis, we investigated two separate instability mechanisms that can lead to the formation of quantum dots. The mechanism in Chapter 2 induced the instability of the film free surface as a result of strong surface-energy anisotropy coupled with wetting interactions between the film and the substrate. According to this mechanism, the substrate determines the initial crystallographic orientation of the film surface which, due to large surface-energy anisotropy, can be thermodynamically unstable in the absence of the substrate. In this case, when the film grows sufficiently thick and no longer feels the presence of the substrate, it undergoes faceting instability and decomposes into a system of faceted pyramids. In the small-slope approximation, we derived a nonlinear partial differential equation that governs the surface evolution. We showed that wetting interactions between the film and the substrate can suppress the long-wave modes of the faceting instability and change the spectrum from long-wave to short-wave, leading to the possibility of the formation of stable regular arrays of quantum dots. We investigated this possibility both analytically and numerically. We performed a weakly nonlinear analysis and derived a system of amplitude equations describing the film evolution near the instability threshold. We found that, near the instability threshold, the formation of stable hexagonal arrays of quantum dots is possible.

In Chapter 3, we studied the Asaro-Tiller-Grinfeld instability in the presence of wetting interactions. In this case, we showed that the stress balance boundary conditions of

the corresponding elasticity problem must include an additional term that describes the *wetting stress*. We determined the steady-state solution of the elasticity problem, studied its stability, and found that the wetting stress breaks the symmetry between the tensile and compressive epitaxial strains. We then solved the elasticity problem in the long-wave approximation and derived a nonlocal integro-differential equation governing the evolution of the film surface. To study the possibility of the formation of spatially-regular dot arrays, we performed linear and weakly nonlinear analyses and showed that, in the case of two-layer and glued-layer wetting potentials, such arrays result from a subcritical bifurcation and are therefore unstable. We also performed numerical simulations of the nonlocal integro-differential equation and studied the evolution of quantum dots. We showed that, after formation, the dots undergo coarsening with larger islands growing at the expense of smaller ones, and we characterized the coarsening kinetics by different parameters.

Finally in Chapter 4, we investigated the dynamics of a crystalline surface growing by step-flow governed by Lévy flights. We developed the analog of the Burton, Cabrera, Frank theory for the case of Lévy flights. For the quasistationary and full problems, we found analytical expressions for the adatom density between two steps as well as the step flow velocity as a function of the terrace length. In both cases, as compared to normal diffusion, Lévy flights resulted in denser adatom profiles with wider and flatter maximums due to the lower probability of adatoms reaching a step. We also determined the asymptotics of the step flow for large terrace length and found the saturation velocity as a function of the anomalous diffusion exponent.

References

[1] R. J. Asaro and W. A. Tiller, "Interface morphology development during stress-corrosion cracking via surface diffusion," *Metallurgical Transactions*, vol. 3, pp. 1789–&, 1972.

[2] M. Y. Grinfeld, "Instability of the separation boundary between a non-hydrostatically stressed elastic body and a melt," *Soviet Physics - Doklady*, vol. 31, pp. 831–834, 1986.

[3] P. Liu, Y. W. Zhang, and C. Lu, "Coarsening kinetics of heteroepitaxial islands in nucleationless Stranski-Krastanov growth," *Physical Review B*, vol. 68, p. 035402, 2003.

[4] V. A. Shchukin and D. Bimberg, "Spontaneous ordering of nanostructures on crystal surfaces," *Reviews of Modern Physics*, vol. 71, pp. 1125–1171, 1999.

[5] B. J. Spencer, P. W. Voorhees, and S. H. Davis, "Morphological instability in epitaxially strained dislocation-free solid films," *Physical Review Letters*, vol. 67, pp. 3696–3699, 1991.

[6] D. J. Srolovitz, "On the stability of surfaces of stressed solids," *Acta Metallurgica*, vol. 37, pp. 621–625, 1989.

[7] Y. W. Zhang, "Self-organization, shape transition, and stability of epitaxially strained islands," *Physical Review B*, vol. 61, pp. 10388–10392, 2000.

[8] Y. W. Zhang and A. F. Bower, "Three-dimensional analysis of shape transitions in strained-heteroepitaxial islands," *Applied Physics Letters*, vol. 78, pp. 2706–2708, 2001.

[9] D. Moldovan and L. Golubovic, "Interfacial coarsening dynamics in epitaxial growth with slope selection," *Physical Review E*, vol. 61, pp. 6190–6214, 2000.

[10] M. Siegert, "Coarsening dynamics of crystalline thin films," *Physical Review Letters*, vol. 81, pp. 5481–5484, 1998.

[11] M. Siegert and M. Plischke, "Slope selection and coarsening in molecular-beam epitaxy," *Physical Review Letters*, vol. 73, pp. 1517–1520, 1994.

[12] P. Smilauer, M. Rost, and J. Krug, "Fast coarsening in unstable epitaxy with desorption," *Physical Review E*, vol. 59, pp. R6263–R6266, 1999.

[13] F. M. Ross, J. Tersoff, and R. M. Tromp, "Coarsening of self-assembled Ge quantum dots on Si(001)," *Physical Review Letters*, vol. 80, pp. 984–987, 1998.

[14] K. Alchalabi, D. Zimin, G. Kostorz, and H. Zogg, "Self-assembled semiconductor quantum dots with nearly uniform sizes," *Physical Review Letters*, vol. 90, p. 026104, 2003.

[15] C. D. Rudin and B. J. Spencer, "Equilibrium island ridge arrays in strained solid films," *Journal of Applied Physics*, vol. 86, pp. 5530–5536, 1999.

[16] A. A. Golovin, S. H. Davis, and A. A. Nepomnyashchy, "Model for faceting in a kinetically controlled crystal growth," *Physical Review E*, vol. 59, pp. 803–825, 1999.

[17] A. A. Golovin, A. A. Nepomnyashchy, S. H. Davis, and M. A. Zaks, "Convective Cahn-Hilliard models: From coarsening to roughening," *Physical Review Letters*, vol. 86, pp. 1550–1553, 2001.

[18] T. V. Savina, A. A. Golovin, S. H. Davis, A. A. Nepomnyashchy, and P. W. Voorhees, "Faceting of a growing crystal surface by surface diffusion," *Physical Review E*, vol. 67, p. 021606, 2003.

[19] C. H. Chiu, "Stable and uniform arrays of self-assembled nanocrystalline islands," *Physical Review B*, vol. 69, p. 165413, 2004.

[20] A. A. Golovin, S. H. Davis, and P. W. Voorhees, "Self-organization of quantum dots in epitaxially strained solid films," *Physical Review E*, vol. 68, p. 056203, 2003.

[21] H. R. Eisenberg and D. Kandel, "Origin and properties of the wetting layer and early evolution of epitaxially strained thin films," *Physical Review B*, vol. 66, p. 155429, 2002.

[22] H. R. Eisenberg and D. Kandel, "Wetting layer thickness and early evolution of epitaxially strained thin films," *Physical Review Letters*, vol. 85, pp. 1286–1289, 2000.

[23] T. V. Savina, P. W. Voorhees, and S. H. Davis, "The effect of surface stress and wetting layers on morphological instability in epitaxially strained films," *Journal of Applied Physics*, vol. 96, pp. 3127–3133, 2004.

[24] M. Ortiz, E. A. Repetto, and H. Si, "A continuum model of kinetic roughening and coarsening in thin films," *Journal of the Mechanics and Physics of Solids*, vol. 47, pp. 697–730, 1999.

[25] P. Nozieres, *Solids far from Equilibrium*. Cambridge University Press, 1992.

[26] A. Pimpinelli and J. Villain, *Physics of Crystal Growth*. Cambridge University Press, 1998.

[27] B. J. Spencer, P. W. Voorhees, and S. H. Davis, "Morphological instability in epitaxially strained dislocation-free solid films–linear-stability theory," *Journal of Applied Physics*, vol. 73, pp. 4955–4970, 1993.

[28] M. E. Gurtin, *Thermomechanics of Evolving Phase Boundaries in the Plane*. Clarendon, Oxford, 1993.

[29] J. Stewart and N. Goldenfeld, "Spinodal decomposition of a crystal-surface," *Physical Review A*, vol. 46, pp. 6505–6512, 1992.

[30] C. H. Chiu and H. Gao, *Thin Films: Stresses and Mechanical Properties V*, p. 33. Materials Research Society, 1995.

[31] M. J. Beck, A. van de Walle, and M. Asta, "Surface energetics and structure of the Ge wetting layer on Si(100)," *Physical Review B*, vol. 70, p. 205337, 2004.

[32] J. Tersoff, "Stress-induced layer-by-layer growth of Ge on Si(100)," *Physical Review B*, vol. 43, pp. 9377–9380, 1991.

[33] B. J. Spencer, "Asymptotic derivation of the glued-wetting-layer model and contact-angle condition for Stranski-Krastanow islands," *Physical Review B*, vol. 59, pp. 2011–2017, 1999.

[34] Z. G. Suo and Z. Y. Zhang, "Epitaxial films stabilized by long-range forces," *Physical Review B*, vol. 58, pp. 5116–5120, 1998.

[35] F. Liu and H. Metiu, "Dynamics of phase-separation of crystal-surfaces," *Physical Review B*, vol. 48, pp. 5808–5817, 1993.

[36] D. Walgraef, *Spatio-Temporal Pattern Formation*. Springer, New York, 1997.

[37] P. C. Matthews and S. M. Cox, "Pattern formation with a conservation law," *Nonlinearity*, vol. 13, pp. 1293–1320, 2000.

[38] A. A. Golovin, M. S. Levine, T. V. Savina, and S. H. Davis, "Faceting instability in the presence of wetting interactions: A mechanism for the formation of quantum dots," *Physical Review B*, vol. 70, p. 235342, 2004.

[39] R. B. Hoyle, G. B. McFadden, and S. H. Davis, "Pattern selection with anisotropy during directional solidification," *Philosophical Transactions of the Royal Society of London Series A–Mathematical Physical and Engineering Sciences*, vol. 354, pp. 2915–2949, 1996.

[40] G. Springholz, V. Holy, M. Pinczolits, and G. Bauer, "Self-organized growth of three-dimensional quantum-dot crystals with fcc-like stacking and a tunable lattice constant," *Science*, vol. 282, pp. 734–737, 1998.

[41] J. A. Floro, M. B. Sinclair, E. Chason, L. B. Freund, R. D. Twesten, R. Q. Hwang, and G. A. Lucadamo, "Novel SiGe island coarsening kinetics: Ostwald ripening and elastic interactions," *Physical Review Letters*, vol. 84, pp. 701–704, 2000.

[42] V. A. Shchukin, D. Bimberg, T. P. Munt, and D. E. Jesson, "Stability of an hexagonal array of coherently strained conical islands against Ostwald ripening," *Annals of Physics*, vol. 320, pp. 237–256, 2005.

[43] V. Holy, G. Springholz, M. Pinczolits, and G. Bauer, "Strain induced vertical and lateral correlations in quantum dot superlattices," *Physical Review Letters*, vol. 83, pp. 356–359, 1999.

[44] G. Springholz, "Three-dimensional stacking of self-assembled quantum dots in multilayer structures," *Comptes Rendus Physique*, vol. 6, pp. 89–103, 2005.

[45] H. R. Eisenberg and D. Kandel, "Formation, ripening, and stability of epitaxially strained island arrays," *Physical Review B*, vol. 71, p. 115423, 2005.

[46] W. T. Tekalign and B. J. Spencer, "Evolution equation for a thin epitaxial film on a deformable substrate," *Journal of Applied Physics*, vol. 96, pp. 5505–5512, 2004.

[47] Y. Xiang and W. N. E, "Nonlinear evolution equation for the stress-driven morphological instability," *Journal of Applied Physics*, vol. 91, pp. 9414–9422, 2002.

[48] Y. Y. Pang and R. Huang, "Nonlinear effect of stress and wetting on surface evolution of epitaxial thin films," *Physical Review B*, vol. 74, p. 075413, 2006.

[49] D. J. Seol, S. Y. Hu, Z. K. Liu, L. Q. Chen, S. G. Kim, and K. H. Oh, "Phase-field modeling of stress-induced surface instabilities in heteroepitaxial thin films," *Journal of Applied Physics*, vol. 98, p. 044910, 2005.

[50] S. M. Wise, J. S. Lowengrub, J. S. Kim, K. Thornton, P. W. Voorhees, and W. C. Johnson, "Quantum dot formation on a strain-patterned epitaxial thin film," *Applied Physics Letters*, vol. 87, p. 133102, 2005.

[51] L. D. Landau and E. M. Lifshits, *Elasticity Theory*. Pergamon Press, 1981.

[52] S. M. Cox and P. C. Matthews, "Instability and localisation of patterns due to a conserved quantity," *Physica D-Nonlinear Phenomena*, vol. 175, pp. 196–219, 2003.

[53] M. C. Cross and P. C. Hohenberg, "Pattern-formation outside of equilibrium," *Reviews Of Modern Physics*, vol. 65, pp. 851–1112, 1993.

[54] W. K. Burton, N. Cabrera, and F. C. Frank, "The growth of crystals and the equilbrium structure of the surfaces," *Philosophical Transactions of the Royal Society of London Series A–Mathematical and Physical Sciences*, vol. 243, pp. 299–358, 1951.

[55] R. Metzler and J. Klafter, "The random walk's guide to anomalous diffusion: A fractional dynamics approach," *Physics Reports*, vol. 339, pp. 1–77, 2000.

[56] S. Havlin and D. Ben-Avraham, "Diffusion in disordered media," *Advances in Physics*, vol. 36, pp. 695–798, 1987.

[57] M. F. Shlesinger, B. J. West, and J. Klafter, "Lévy dynamics of enhanced diffusion: Application to turbulence," *Physical Review Letters*, vol. 58, pp. 1100–1103, 1987.